FAILURE ANALYSIS OF GREEN CERAMIC BODIES DURING THERMAL DEBINDING

A Thesis

Presented to

The Faculty of the Graduate School

at the University of Missouri-Columbia

In Partial Fulfillment

of the Requirements for the Degree

Master of Science

---

by

Rajiv M. Sachanandani

Dr. Stephen J. Lombardo, Thesis Supervisor

July 2009

The undersigned, appointed by the Dean of the Graduate School, have examined the thesis entitled

FAILURE ANALYSIS OF GREEN CERAMIC BODIES DURING THERMAL DEBINDING

Presented by

Rajiv M. Sachanandani

A candidate for the degree of

Master of Science

And hereby certify that in their opinion, it is worthy of acceptance.

Dr. Stephen J. Lombardo _____

Dr. Qingsong Yu _____

Dr. Frank Z. Feng _____

ACKNOWLEDGEMENTS

I would like to take this opportunity to thank Dr. Stephen J. Lombardo who has guided me through the completion of my graduate studies in University of Missouri. I would like to thank him for the enormous patience he has shown with me throughout the course of my graduate studies. Of the many valuable things I have learned from him, the most important are critical analysis and problem solving, which I intend to apply in my everyday life.

I would like to sincerely thank the members of my thesis committee; Dr. Qingsong Yu and Dr. Frank Z. Feng for giving very valuable reviews regarding my thesis and regarding the presentation of my research.

I would like to thank all my colleagues who have helped me throughout my graduate studies. I would like to first thank Dr. Jeong Woo Yun who patiently taught me all the experiments and would always answer my questions. I would also like to thank Andrew Ritts, Kumar Krishnamurthy, Matt Schurwanz, Brandon Abeln and Simit Patel for their help, and support. I whole-heartedly thank Rita Preckshot for all the help she gave me for making my graduate study in the United States more comfortable. I sincerely thank my family back in India whose constant support and encouragement helped me successfully complete my graduate studies in the United States

FAILURE ANALYSIS OF GREEN CERAMIC BODIES DURING THERMAL DEBINDING

Rajiv M Sachanandani

Dr. Stephen J. Lombardo Thesis Supervisor

ABSTRACT

During the processing of multilayer ceramic capacitors (MLCs), binders (polymers) are often added to increase the strength of the green body. These binders need to be removed prior to densification of the ceramic components. Binders are commonly removed by oxidation in air by subjecting the green body to heating cycles. The specification of thermal debinding cycle is a difficult problem and often leads to the failure of green body, due to inappropriate scheduling of the heating cycle. In order to develop optimum heating cycles, it is important to have an understanding of the failure behavior of green body during thermal debinding.

MLC green bodies, with barium titanate as the dielectric and poly(vinyl butyral) and butyl benzyl phthalate as the main components of the binder, have been subjected to rapid heating cycles in order to cause failure. Two methods were used in order to determine the failure conditions of the green bodies. In one approach, the heating rate was held constant and the dimensions of the green bodies were varied, while in the second method, the size of the green body was held constant and the heating rate was varied. In all cases, failure of the green body occurred between 115-140°C. Models showed that at the time of sample failure, binder loading was high and the pressure in the center of the green body was nearly constant, independent of the method used to cause the samples to fail. The internal pressure was then used with a previously developed algorithm to develop rapid debinding cycles without causing component failure.

Based on the results of previous work, relationships between spatial pressure distribution and spatial stress distribution are presented. Models for predicting the strength of the green body throughout the thermal debinding cycle were developed. The strength of the green body, the stress distribution and the internal pressure distribution were then related. Based on the combination of the results from the strength, pressure, and stress models qualitative assessments were made on how these important quantities are changing relative to each other during thermal debinding and how they influence the failure behavior. Furthermore, the tensile properties of the green ceramic tapes at different binder loadings and the binder system alone were studied.

TABLE OF CONTENTS

LIST OF TABLES

TABLE

LIST OF FIGURES

FIGURES

CHAPTER 1

INTRODUCTION

In industry, thermal debinding is the traditional mode of binder removal from multilayer ceramic capacitors (MLCs). Binder removal from ceramics takes as long as 50-150 h, thereby contributing significantly to the manufacturing costs and also controlling the production rate. Increasing energy costs and demand for multilayer ceramic capacitors calls for the development of rapid binder removal cycles. These cycles should not only be fast but also result in a defect free ceramic capacitor. Defect formation, which arises from excessive stresses, plays a major role in determining the duration of the heating cycle. This thesis presents failure behavior of green MLCs as a function of changing body size and heating rate. This is then used to design rapid heating cycles. Furthermore, models are presented to qualitatively analyze the failure behavior in terms of the stresses and strength of the green body.

1.1 MANUFACTURING OF MULTILAYER CERAMIC CAPACITORS (MLCs)

In industry, multilayer ceramic capacitor are produced in various steps and these are illustrated in figure 1.1. The first step in the processing is the preparation of a suitable slurry [1], which is achieved by mixing the raw materials comprised of ceramic powder, binder, plasticizer, solvents, and other organic additives. Nonaqueous slurries are commonly used because of the ease of powder dispersion and slurry drying. The ceramic slurry is then tape casted on a clean, smooth, impervious surface such as Mylar. The thickness of the tape can be varied by changing the height of the doctor blade above the surface. After casting, the ceramic tape, which is in "green state" (terminology used to identify products before sintering), is allowed to dry completely. Then, the dry green ceramic tapes are screen printed with electrodes. In screen printing, an open pattern in a stencil defines the pattern printed on the green ceramic tape. After electrode printing, these tapes are cut, stacked, and laminated at 50-80°C and 3-30 MPa.

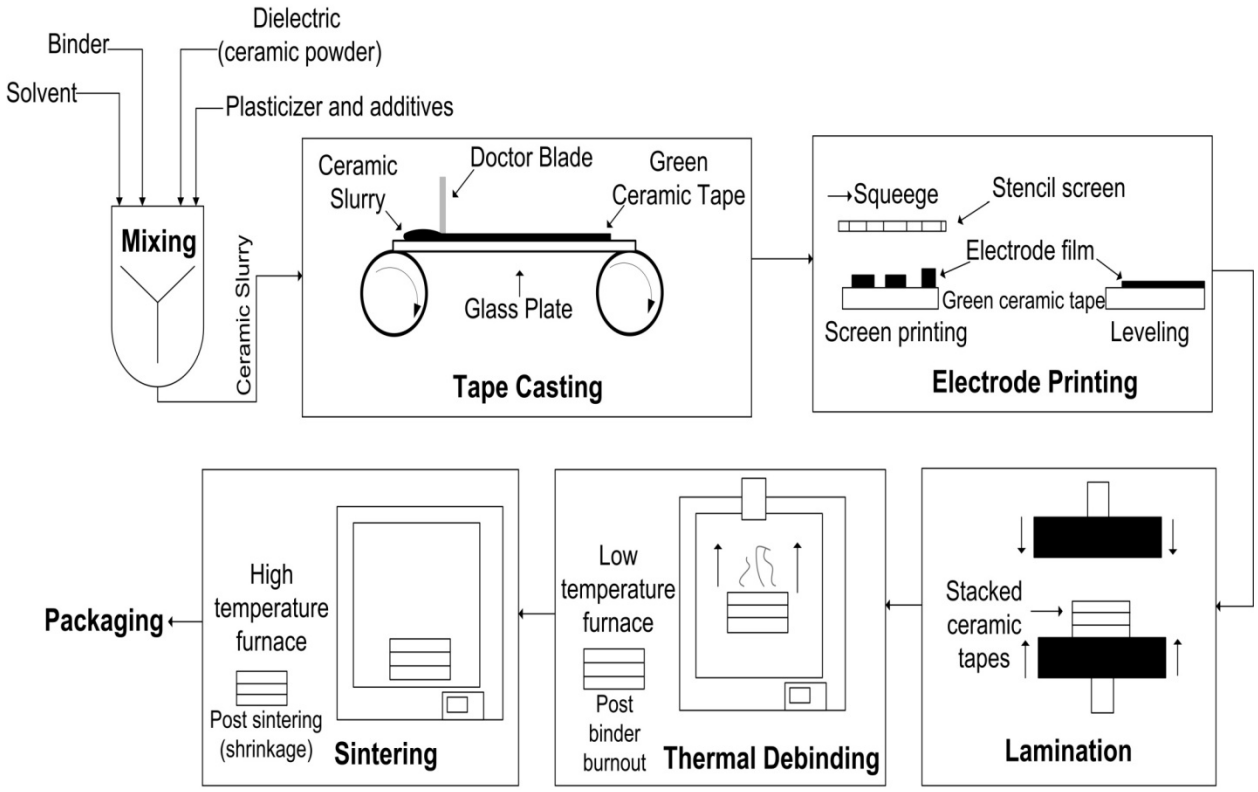

Figure 1.1: Steps involved in the processing of multilayer ceramic capacitors.

Next, the green MLCs are subjected to heating cycles in a low temperature furnace (up to 800°C), where the binder, plasticizer, and other organic additives are removed by decomposition into the gaseous phase. This stage of the MLC processing is a crucial stage, as inappropriate scheduling of heating cycle can lead to failure. To avoid this in industry, long cycles are used. After binder removal, the weak green body is then sintered in a high temperature furnace (up to 2200°C). Sintering is essentially the densification of ceramic objects to obtain high strength. After sintering, the MLC is sent for packaging.

1.2 FAILURE BEHAVIOR OF GREEN BODIES DURING BINDER REMOVAL

The development of rapid binder removal [2,3] cycles is a difficult problem. Heat transfer, decomposition reactions, and mass transfer all occur simultaneously, which contributes to the difficulty. These simultaneous processes give rise to internal pressure distribution [4] in the porous ceramic bodies. This, in turn, cause stresses within the skeletal network. When these stresses exceed the strength of the body, the green ceramic component experiences failure either by cracks, delamination or even by complete fracture. An example of failure by delamination during binder removal and an example of successful binder removal is shown in figure 1.2.

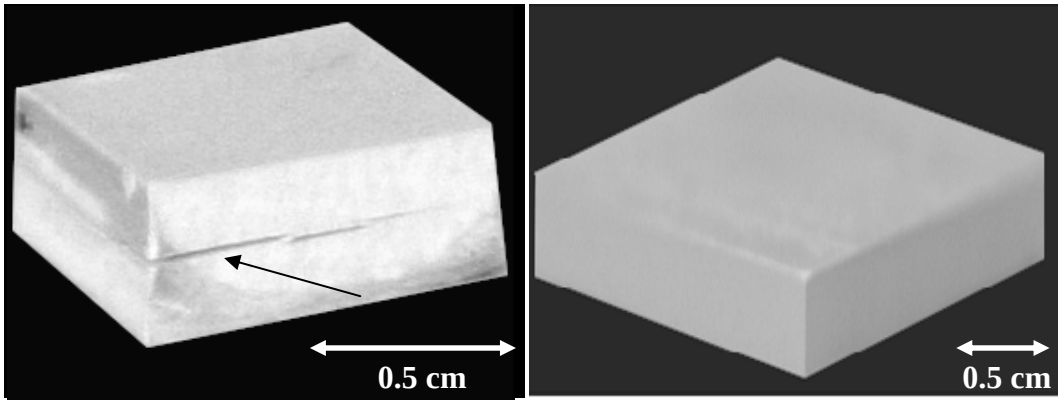

Figure 1.2: Image of green multilayered ceramic body which failed by delamination and ceramic body which survived the binder removal heating cycle.

In earlier work [5,6], variational calculus has been used to determine minimum time heating cycle (MTHC) for thermal debinding. The variational calculus model is based upon the solution to a three-dimensional convective transport equation that describes flow in porous media arising from the thermal decomposition of binder. Two of the inputs to the model are the failure

conditions (failure temperature and failure pressure) of the green body. Therefore, it becomes imperative to have an understanding of the failure behavior of the green body.

It is the major aim of this work to study the failure behavior of the green bodies with respect to dimensions of the green body and the heating rate used in the debinding cycle. The effects of these two circumstances on the minimum time heating cycle are investigated. To have a further insight on failure, we have developed models for the strength [7-9] of the green body during the binder removal heating cycle. These strength models are then studied along with the stress distribution [10] obtained from the finite element analysis data from previous work.

1.3 THESIS ORGANIZATION

In Chapter 2 multilayer ceramic green bodies have been subjected to rapid heating cycles in order to cause failure to occur. In one approach, the heating rate was held constant and the dimensions of the green bodies were varied, while in the second method, the size of the green body was held constant and the heating rate was varied. The results obtained from the above experiments are then used in models to determine the binder loading and the internal pressure in the center of the green body at failure. The internal pressure was then used as an input into a previously developed algorithm in order to develop rapid debinding cycles without causing component failure.

To have a better understanding of the failure behavior during thermal debinding, Chapter 3 presents relationships between internal pressure, stress, and strength of green body. The pressure distribution in the green body is first translated into a stress distribution. Models are then used to predict the strength of green body. For the two cases of imposed failure presented in Chapter 2, stress-strength plots are used to get a qualitative understanding of when failure occurs during the binder removal process.

As mentioned in Chapter 3, the lack of knowledge of stress-strain behavior and strength of green bodies had lead us to conduct preliminary experiments for the tensile properties of the binder system and green body at different binder loadings and at room temperature. The results of these experiments are presented in Chapter 4

1.4 REFERENCES

1. J. S. Reed, "Principles of Ceramics Processing," Wiley-Interscience Publications, New York 525-594 (1995).
2. R. M. German, "Theory of Thermal Debinding," *Int. J. Powder Metall.*, **23**[4], 237-45 (1987).
3. J. A. Lewis, "Binder Removal From Ceramics," *Annual Rev. Mater. Sci.*, **27**, 147-173 (1997).
4. K. Feng and S. J. Lombardo, "Modeling of the Pressure Distribution in Three-Dimensional Porous Green Bodies during Binder Removal," *J. Am. Ceram. Soc.,* **86,** 234-40 (2003).
5. S. J. Lombardo and Z. C. Feng, "Analytic Method for the Minimum Time for Binder Removal from Three-Dimensional Porous Green Bodies," *J. of Mat. Res.,* **18,** 2717-2723 (2003).
6. S. J. Lombardo and Z. C. Feng, "Determination of the Minimum Time for Binder Removal and Optimum Geometry for Three-Dimensional Porous Green Bodies," *J. Am. Ceram. Soc.,* **6** [12], 2087-2092 (2003).
7. H. Rumpf, "The Strength of Granules and Agglomerates: International Symposium on Agglomeration", Interscience, London, UK, 1962.
8. G. Onoda, "Theoretical Strength of Dried Green Bodies with Organic Binders," *J. Am. Ceram. Soc.,* **59** [5], 236-239 (1976).
9. S. A. Uhland, R. K. Holman, S. Moissette, M. J. Cima, and E. M. Sachs, "Strength of Green Ceramics with Low Binder Content," *J. Am. Ceram. Soc.,* **84** [12], 2809-2818 (2001).
10. Z. C. Feng, B. He, and S. J. Lombardo, "Stress Distribution in Porous Ceramic Bodies During Binder Burnout," *J. Appl Mech.*, **69,** 497-501 (2002).

CHAPTER 2

THE EFFECT OF GREEN BODY SIZE AND HEATING RATE ON FAILURE DURING THERMAL DEBINDING AND ON DEBINDING CYCLE TIME

2.1 INTRODUCTION

In the processing of green ceramic components, binders are often used to impart mechanical strength for handling, and, furthermore, may be added to aid in subsequent processing steps such as in the lamination of green ceramic tapes. The binders, which may consist of one or more organic components, also influence the process of thermal debinding [1,2], for not only does binder occupy pore space, and thus reduce the gas permeability of the green body, but the mechanical properties of the binder may be responsible in part or in whole for the conditions at which and the manner in which the green body fails.

During the thermal debinding cycle, the green body will fail when the local stress [3-5] arising from the distribution of pressure [3-10] within the green body exceeds the local strength. The pressure distribution, however, is a complex, coupled function of the temperature distribution in the green body, the decomposition kinetics of the binder, and the gas permeability of the green body, all of which are changing with time. Because the pressure distribution arises not as an external applied force but rather as an internal body force, the failure behavior of green ceramic components becomes difficult to probe by traditional testing methods.

To circumvent this difficulty and yet still be able to provide some insight into the failure behavior of green bodies during thermal debinding [11-16], two procedures may be used instead. In one case, green bodies of different size may be fabricated and then subjected to rapid debinding cycles at a constant heating rate. Such a procedure may be relevant to scale-up, whereby a heating cycle is first developed for a small test sample, but the ultimate component size will be larger. In a second procedure, green bodies of constant size may be fabricated, which are then subjected to rapid debinding cycles at different heating rates. This approach may be relevant for complex-shaped components, where the expense of a mold or die precludes the

fabrication of green bodies of different dimensions. Regardless of which procedure is used, however, it is of interest to know if the green bodies will fail at the same temperature, at the same internal pressure, or at the same volume fraction of binder. Thus, one aim of this work is to present experimental data on the failure temperature of green bodies subjected to these two types of debinding procedures.

In earlier work [10,17], we have developed a methodology based on variational calculus to determine the minimum time heating cycle (MTHC) for thermal debinding from open pore compacts. The methodology consists of determining the physical attributes of the green body, the decomposition kinetics of the binder, the permeability of the green body, and the temperature at which the green body fails. This latter quantity can be determined in different ways, two of which are mentioned above. A second aim of this work is thus to use the failure temperatures of green bodies subjected to these two debinding procedures, along with models, to assess the values of other difficult to measure parameters at failure such as the volume fraction of binder and the internal pressure. Finally, the differences in failure behavior of green bodies subjected to the two debinding procedures can then be used to assess the uniqueness of the MTHCs determined from the variational calculus algorithm.

2.2 EXPERIMENTAL

Green ceramic tapes were prepared from barium titanate powder (Tamtron X7R 422H, Ferro Electronic Materials, Niagara Falls, NY), which has a mean particle diameter of 1.1 □m and specific surface area of 3.0 m^2/g. A slurry was prepared at 65 weight% powder with 35 weight% binder solution consisting of 14.5 weight% poly(vinyl butyral) binder (Butvar B98, Richard E. Mistler, Inc., Yardley PA), 10.9% butyl benzyl phthalate plasticizer (Santicizer 160, Richard E. Mistler, Inc.) and 3.8% blown Menhaden fish oil (Z-3, Richard E. Mistler, Inc.) in a mixture of 35.4% each of xylene and ethanol. After ball milling, the slurry was de-aired and then filtered through a 53 μm nylon mesh. The slurry was then tape cast with a single stationary doctor blade on a Mylar carrier film. After drying, the thickness of the tapes was approximately 150-160 μm. The total organic content of the substrates was 10.8% by weight, as determined by thermal gravimetry in air. The dried tapes were stacked and laminated in a press at 7 MPa and 85°C for 10 min and then cut into parallelepipeds of different dimensions.

To obtain the temperature, T_f, at which failure of the green body occurs, the front door of the box furnace was replaced with a thermally resistant window. The green components were then placed in the furnace in air and subjected to rapid linear heating rates. In addition to visual observation of the samples, a 6 megapixel digital camera (Canon EOS 10D, Lake Success, New York) was used to take images of the samples at 1°C intervals with a remote timer (Canon TC-80N3).

2.3 MODEL

Because the model and governing equations have been derived and presented in detail elsewhere, we will only succinctly summarize the relevant equations here along with references to the earlier work. The rate of binder decomposition, r, can be represented as

$$r = -\frac{d\varepsilon_b}{dt} = A\exp\left[-\frac{E}{RT}\right]\varepsilon_b \qquad 1$$

where t is the time, A is the preexponential factor, E is the activation energy, T is the temperature, R is the gas constant, and ε_b is the volume fraction of binder. The solution to Eq. 1, for a linear heating rate, β, is [18]

$$\frac{\varepsilon_b}{\varepsilon_{bo}} = \exp\left[-\frac{A}{\beta}\left\{\frac{\left(\frac{RT^2}{E}\right)\exp\left(-\frac{E}{RT}\right)}{1+\frac{2RT}{E}} - \frac{\left(\frac{RT_o^2}{E}\right)\exp\left(-\frac{E}{RT_o}\right)}{1+\frac{2RT_o}{E}}\right\}\right] \qquad 2$$

where $\varepsilon_{b,o}$ is the initial volume fraction of binder and T_o is the initial temperature.

During the thermal debinding heating cycle, the normalized pressure in the center of the green body, $(P/P_o)_o$, is given by [19]

$$\left(\frac{P}{P_o}\right)_o \approx \left(1+0.8365\frac{L_x^2}{2\rho_o^2\kappa_x}\frac{\mu}{R}\frac{r\rho_b}{M}\frac{T}{T_o^2}\frac{W^2H^2}{W^2H^2+W^2+H^2}\right)^{1/2} \qquad 3a$$

$$= \left(1+G\frac{rT}{\kappa_x}\right)^{1/2} \qquad 3b$$

The stretched dimensionless lengths, W and H, of the green body are in terms of the dimensions L_x , L_y, and L_z, of the component as given by

$$W = \sqrt{\frac{\kappa_x}{\kappa_y}}\frac{L_y}{L_x};\ H = \sqrt{\frac{\kappa_x}{\kappa_z}}\frac{L_z}{L_x} \qquad 4$$

The permeability, κ, of the body is taken as anisotropic and is given in the *i*th direction by

$$\kappa_i = \frac{\varepsilon^3}{k(1-\varepsilon)^2 S^2} \qquad 5$$

where ε is the porosity, S is the specific surface, and k is a constant. The volume fractions of binder, porosity, and ceramic, ε_c, are related by

$$\varepsilon_b + \varepsilon + \varepsilon_c = 1 \qquad 6$$

The quantity G in Eq. 3b is a constant given by

$$G = 0.8365\frac{\mu\rho_b L_x^2}{2\rho_o^2 RMT_o^2}\frac{W^2H^2}{W^2H^2 + W^2 + H^2} \qquad 7$$

where M is the molecular weight of the gas decomposition species and ρ is the density, and the subscripts b and o denote binder and initial gas conditions in the furnace, respectively.

When Eq. 3 is used to determine the threshold pressure, $P_t=(P/P_o)_o$, at which the green body fails, then the following holds

$$P_t = \left(1 + G\frac{r_f T_f}{\kappa_{xf}}\right)^{1/2} \qquad 8$$

where subscript f denotes the value of a quantity at the failure temperature, T_f. In light of this, P_t is thus also a value, which will ultimately be used to determine the MTHC. The minimum debinding cycle time, t^*, is obtained by variational calculus, as described elsewhere [9,10], by rearranging and integrating Eq. 1 to yield:

$$t^* = \int_0^{\varepsilon_{bo}} \frac{d\varepsilon_b}{r} \qquad 9$$

which when combined with Eq. 3b yields

$$t^* = \int_0^{\varepsilon_{bo}} \frac{GT}{\kappa_x \left[\left(\frac{P}{P_o} \right)_o^2 - 1 \right]} d\varepsilon_b \qquad 10$$

When the value in brackets is set to the constraint that the pressure inside the green body not exceed P_t as given by Eq. 8, then the minimum time becomes

$$t^* = \int_0^{\varepsilon_{bo}} \frac{T}{\kappa_x \left[\frac{r_f T_f}{\kappa_{xf}} \right]} d\varepsilon_b = \frac{T_s}{\left[\frac{r_f T_f}{\kappa_{xf}} \right]} \int_0^{\varepsilon_{bo}} \frac{1}{\kappa_x} d\varepsilon_b \qquad 11$$

where on the right-hand side we have further used the approximation that T=T_s, the start temperature of the heating cycle [9,10]. In this form, Eq. 11 indicates that the minimum time depends directly on the values associated with when the green body fails and on how the permeability evolves during the heating cycle. Although Eq. 11 has no direct dependence on the size of the green body or on the kinetics of binder degradation, these quantities presumably will influence the minimum time heating cycle by the manner in which they influence the values of T_s, r_f, T_f and κ_{xf}. Finally, the evolution of temperature during the MTHC is related to the volume fraction of binder by [9,10]:

$$T(\varepsilon_b) = \frac{-E}{R} \left[\ln \frac{\kappa_x}{\varepsilon_b} \frac{(P_t^2 - 1)}{GT_s A} \right]^{-1} \qquad 12$$

2.4 RESULTS AND DISCUSSION

For the first type of experiment, a multilayer sample was placed in the furnace and heated at a fixed rate of 7.5°C/min; the temperature at which the green body failed was then determined by recording images of the green body within the furnace during the heating cycle. In some instances, it was also possible to observe through the window in real time the occurrence of failure. This procedure was then repeated for other sized samples. Table 2.1 shows that for each body size, the failure temperatures of two replicates are within 3-4°C. With increasing body size, the failure temperature also decreases over a span of approximately 20°C. Figure 2.1 shows images of failed samples of each size. In all cases, the mode of failure is delamination near the mid-plane region of the sample. This location of failure is consistent with the results from earlier modeling work [3,4], which predicts that both the maximum pressure and maximum normal stress occur in the center of the sample.

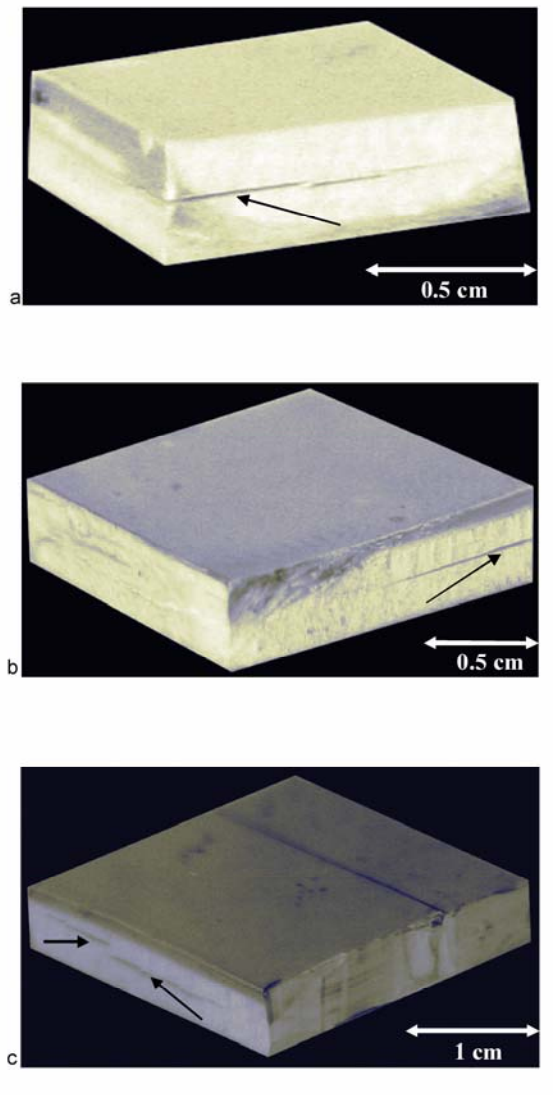

Figure: 2.1: Images of multilayer green ceramic components in the furnace subjected to a linear heating rate of 7.5°C/min. a) Sample A_1 (0.37×1×1 cm) that failed at T_f=136°C b) Sample B_1 (0.42×2×2 cm) that failed at T_f=124°C c) Sample C_1 (0.49×3×3 cm) that failed at T_f=114°C. The locations of delamination are indicated by arrows.

Table 2.1: Failure temperature, binder content at failure, threshold pressure, starting temperature, and minimum time for multilayer samples of different size subjected to a heating rate of 7.5°C/min.

$L_x \times L_y \times L_z$ (cm)	Sample ID (-)	T_f (°C)	ε_{bf} (-)	P_t (-)	T_s (°C)	t^* (h)
0.37×1×1	A_1	136	0.298	1.006	135.2	1.52
	A_2	139	0.298	1.008	138.1	1.32
0.42×2×2	B_1	124	0.299	1.013	123.6	2.73
	B_2	127	0.299	1.015	126.5	2.35
0.49×3×3	C_1	114	0.300	1.016	113.8	4.60
	C_2	118	0.299	1.020	117.7	3.72

For the second type of experiment, samples of a fixed size were subjected to heating rates of 5, 7.5, and 10°C/min, and the temperature at which failure occurred was again recorded. Table 2.2 shows that for each replicate, the samples fail within 3-5°C, and that as the heating rate increases, the failure temperature decreases slightly over approximately 10-15°C. The images in Figure 2.2 show that the mode of failure in all cases again corresponds to delamination near the mid-plane region.

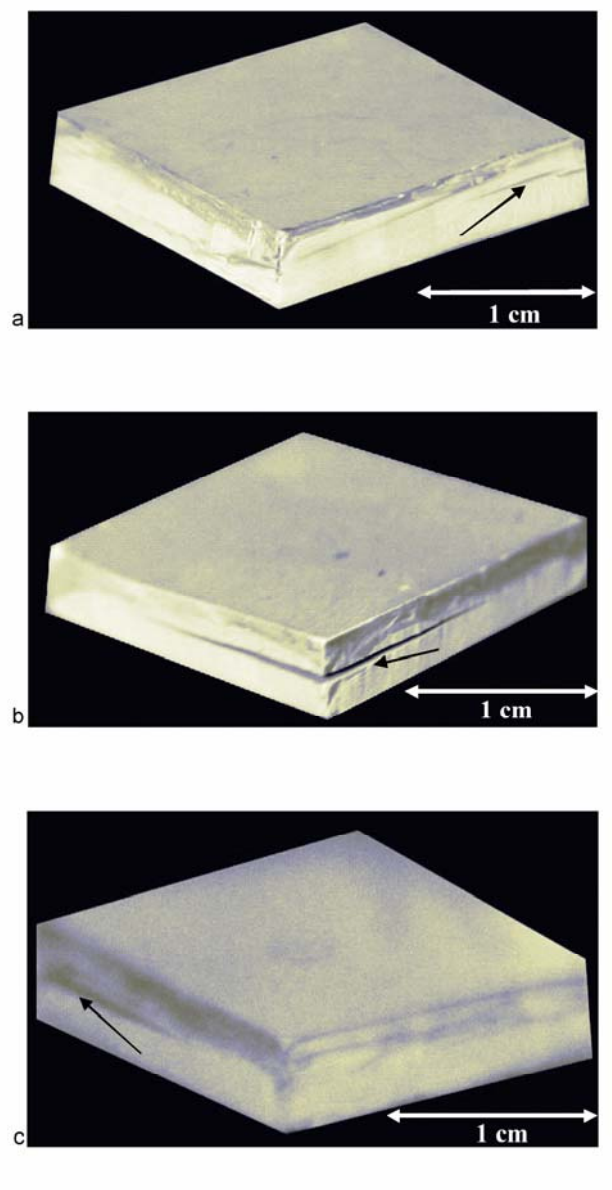

Figure 2.2: Images of multilayer green ceramic components of dimensions 0.42×2×2 cm in the furnace subjected to rapid linear heating rates. a) Sample D_1 heated at 5°C/min that failed at T_f =128°C. b) Sample B_2 heated at 7.5°C/min that failed at T_f =127°C. c) Sample F_1 heated at 10°C/min that failed at T_f=117°C. The locations of delamination are indicated by arrows.

Table 2.2: Failure temperature, binder content at failure, threshold pressure, starting temperature, and minimum time for multilayer samples of 0.42 cm × 2 cm × 2 cm subjected to different heating rates.

β (°C/min)	Sample ID (-)	T_f (°C)	ε_{bf} (-)	P_t (-)	T_s (°C)	t^* (h)
5	D_1	128	0.298	1.016	127.3	2.26
	D_2	131	0.298	1.019	130.1	1.96
7.5	B_1	124	0.299	1.013	123.6	2.73
	B_2	127	0.299	1.015	126.5	2.35
10	F_1	117	0.300	1.009	116.8	3.91
	F_2	122	0.299	1.012	121.7	3.01

To provide some insight into the values of other quantities at the failure temperature, we next use the equations presented earlier to determine the evolution of pressure within the center of body, $(P/P_o)_o$, as a function of the heating cycle. The values of the parameters used in the model are listed in Table 2.3, and all are based upon measured data, as described in more detail in the appendix. Figure 2.3 shows that for components of different size subjected to a fixed heating rate, $(P/P_o)_o$ first increases during the heating cycle as binder is decomposed and then goes through a maximum before decreasing as binder is consumed and more porosity is created within the green body. Figure 2.3 also shows the evolution of binder volume fraction with temperature during the heating cycle. For all three body sizes, the curves of ε_b are identical, which arises from the form of Eq. 2. The increasing branch of the $(P/P_o)_o$ profile corresponds to relatively high binder loading, and the maximum in $(P/P_o)_o$ corresponds to ~17% degradation of the total binder content.

Table 2.3: Parameters used in the simulations in Figures. 2.3-2.7.

Symbol (units)	Value
P_o (MPa)	0.1
T_o (K)	300
M (kg/mol)	0.044
R (m^3 Pa/mol K)	8.314
μ (Pa s)	2.5×10^{-5}
S (m^{-1})	6×10^{5}
k (-)	430
ρ_b (kg/m^3)	1000
ε_s (-)	0.55
ε_{bo} (-)	0.3
ε_o (-)	0.15
S (m^{-1})	6×10^{5}
k (-)	430
κ_y, κ_z (m^2)	$100\times\kappa_x$
ρ_o (mol/m^3)	40.09
A (s^{-1})	1.7×10^{4}
E (J/mol)	68000

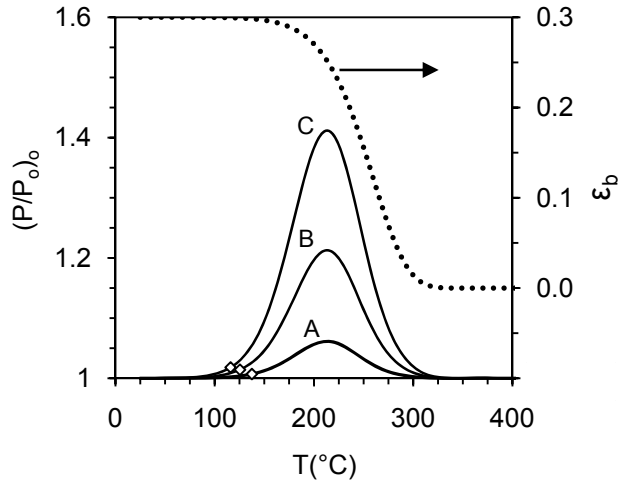

Figure 2.3: Normalized pressure in the body center, $(P/P_o)_o$, and binder volume fraction, ε_b, versus temperature as predicted by the model at a fixed heating rate of 7.5°C/min for samples of different size (A: 0.37×1×1 cm; B: 0.42×2×2 cm; C: 0.49×3×3 cm). The symbols indicate the average temperature in the heating cycle when failure occurred.

Figure 2.4 illustrates how $(P/P_o)_o$ varies with temperature when green bodies of a fixed size are subjected to different heating rates. Now, in contrast to Figure 2.3, the profiles of $(P/P_o)_o$ shift to higher temperature with increasing heating rate, and the overlap in the increasing pressure branch persists to closer to the maxima. The curves of ε_b are now distinct and also shifted to parallel the trends in $(P/P_o)_o$ with heating rate; in all cases, however, the maxima in $(P/P_o)_o$ occur at ~17% of the binder being decomposed.

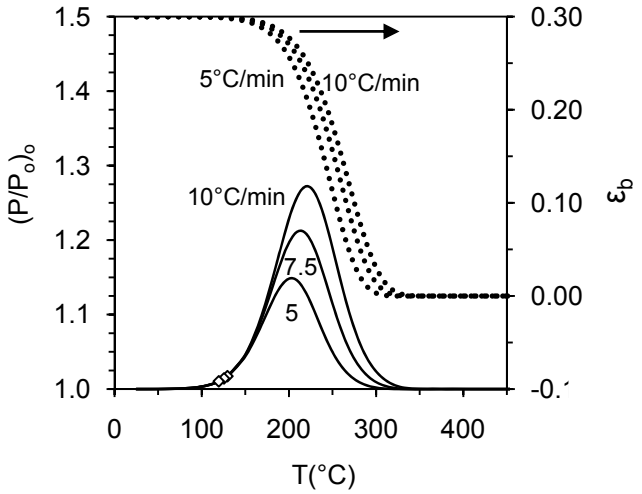

Figure 2.4: Normalized pressure in the body center, $(P/P_o)_o$, and binder volume fraction, ε_b, versus temperature predicted by the model at different heating rates (D: 5°C/min; B: 7.5°C/min; F: 10°C/min) for samples of a fixed size of 0.42×2×2cm. The symbols indicate the average temperature in the heating cycle when failure occurred.

The observed failure temperatures in Tables 2.1 and 2.2 can now be used with Figure. 2.3 and 2.4, along with the model equations used to generate the $(P/P_o)_o$ profiles, to determine values of other quantities at the failure temperature. For example, for green bodies of different dimensions subjected to a constant heating rate, Table 2.1 and Figure 2.3 show that the binder volume fractions at failure are very high and nearly constant, as is P_t. The value of P_t, however, exhibits a ~2% increase with increasing size of the green body. For green bodies of a fixed size subjected to different heating rates, Table 2.2 and Figure 2.4 show that at failure, the binder volume fraction is once again high and nearly constant, and P_t is nearly constant as well. The similarity in the high binder loadings in Tables 2.1 and 2.2 indicates that in all instances, failure occurs at a low value of the gas permeability of the green body.

The results of the two types of failure experiments suggest that for the samples and heating schedules examined here, failure occurs over a narrow range of temperatures with some dependence on either the size of the green body or on heating rate. Thus, the temperature of failure does not appear to be a constant "property," but instead depends on the size of the sample and on the rate at which the sample is heated. In earlier work [16], the effect of increasing body size at a fixed heating rate was also seen to lead to a decrease in the failure temperature, and thus this type of behavior may have general validity. Conversely, no strong trend was indicated for the effect of heating rate on the failure temperature of bodies of constant size in earlier work [17], although the majority of the samples again failed at high binder loading.

In light of the values for T_f and P_t obtained here, we can now address their influence on the minimum time heating cycles. Figure 2.5 shows that for bodies of different size which failed at a fixed heating rate, the MTHC profiles have similar start temperatures, profiles, and duration for the sample replicates. The largest sample has the longest cycle by about a factor of 3 as compared to the smallest sample. In all instances, however, the heating cycles are very short. Figure 2.6 shows the MTHCs determined for samples of fixed size that failed at different heating rates. Once again, the MTHCs for each replicate are fairly similar, whereas the duration of the heating cycles determined for the failure conditions at each heating rate differ by a factor of ~2.

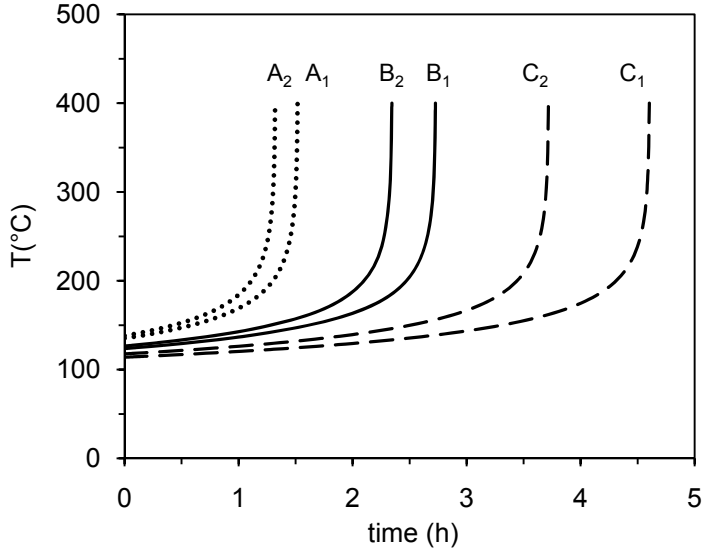

Figure 2.5: Minimum time heating cycles as predicted by the model for samples of different size (A: 0.37×1×1 cm; B: 0.42×2×2 cm; C: 0.49×3×3 cm) which failed at a fixed heating rate of 7.5°C/min.

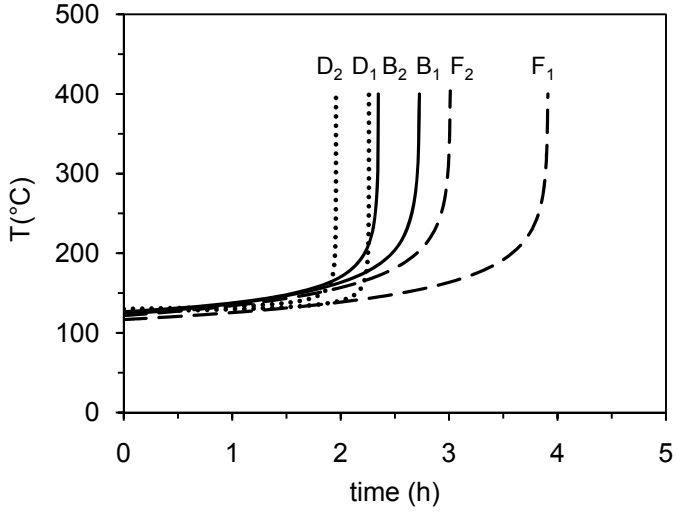

Figure 2.6: Minimum time heating cycles as predicted by the model for the samples of fixed size of 0.42×2×2 cm which failed at different heating rates (D: 5°C/min; B: 7.5°C/min; F: 10°C/min).

The failure temperatures reported in Tables 2.1 and 2.2 and Figures 2.3 and 2.4, although based on observation, have a degree of uncertainty due to the inherent difficulties associated with their method of determination and, furthermore, likely have statistical fluctuation due to sample-to-sample variability. The values of ε_b and P_t, however, are purely calculated quantities and although the underlying parameters in the model have been determined by experiments, measurement errors and approximations in the model equations, combined with the coupling of thermal, kinetic, and transport models, contribute to further uncertainty in their values.

In consideration of all of the coupled uncertainties and approximations mentioned above and in light of the short duration of the heating cycles in Figure. 5 and 6, safety factors, as discussed in more detail elsewhere [20], can next be applied to determine a more conservative debinding cycle. For the MTHC determined for a sample of dimensions 0.42×2×2 cm, multiplicative safety factors of ~2 and ~3.5 were applied to the time, whereas safety factors of 20-25°C were subtracted from the temperature. These more conservative heating cycles were then programmed (see Fig. 7 for an example) into the temperature controller as a series of ramps and holds that closely mimics the underlying more conservative heating cycle. For samples subjected to the heating cycles with safety factors in time of 2 and 20°C in temperature, the green body failed, but the degree of damage to the sample was less than is seen in Figure. 1 and 2. For a safety factor of 3.5 in time and 25°C in temperature, two samples survived this heating schedule with no observed damage (see Figure. 2.8). The MTHC, the more conservative heating cycle, and the heating cycle programmed into the controller are all shown in Fig. 7. For comparison, green multilayer samples of comparable size, composition, and physical properties would require heating cycles of 50-100 h, as compared to the cycle duration of 16 h obtained here.

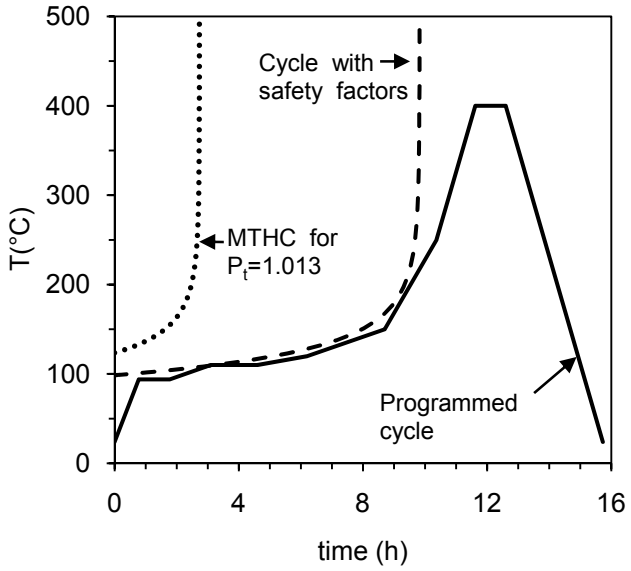

Figure 2.7: The MTHC for sample B_1 and the more conservative heating cycle with a safety factor of 3.5 applied to the time and a safety factor of 25°C applied to the temperature. The cycle programmed into the temperature controller is also shown.

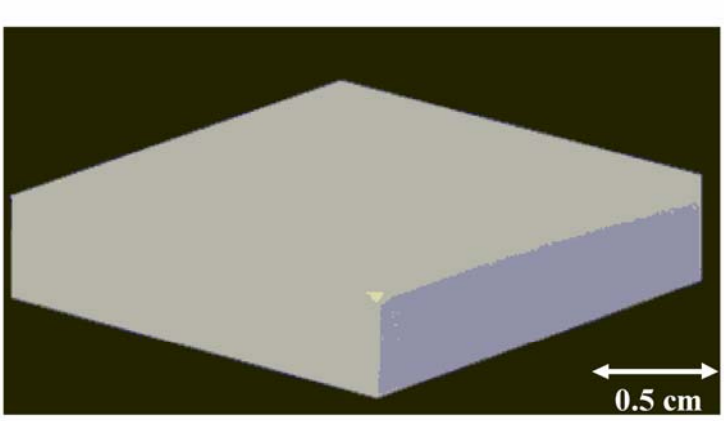

Figure 2.8: Image of a green multilayer ceramic component that survived the programmed heating schedule shown in Figure 2.7.

Based on the results in this study, the green bodies examined here failed over a narrow range of temperature of 20°C, regardless of the component size or the heating rate. Over the same temperature range, the quantities of binder loading and the pressure in the center of the body appear to be nearly constant, although these are computed values and are dependent on all of the coupled assumptions, approximations, and uncertainty in values determined by experiment. Nevertheless, the narrow range over which the green samples fail may suggest that the failure conditions of the green body can be taken as at least approximately constant, and thus a smaller subset of experiments leading to failure of the green body may suffice to establish the MTHC. Then, the use of safety factors can be applied to account for all of the uncertainties, approximations, and variability mentioned above. This procedure is analogous to the use of safety or design factors in component design, whereby a component is only stressed to a fraction of its design strength, and, in fact, this reasoning underlies the rationale for developing the MTHC methodology.

In addition to the specifics of the experimental results presented here on failure behavior, this study also serves to demonstrate a methodology for developing rapid thermal debinding cycles. This procedure, although still having an element of trial-and-error in regards to the determination of the safety factors, leads in relatively few iterations to rapid debinding cycles without introducing defects into the green body. Based on previous work in our lab and in this study, 2-3 iterations with safety factors on time and temperature lead to the desired cycles. This quick convergence on a successful and rapid debinding cycle likely arises because the temperature region of green body failure is first identified, and the MTHC methodology then optimizes the heating cycle using information at the failure temperature. This optimization does not, however, involve the possibly arbitrary specification of ramp rates, hold temperatures, and

hold periods, which taken together may unnecessarily prolong the heating cycle. This careful tailoring of the heating cycle around the temperature region where failure occurs is likely to be difficult to achieve on an *ad hoc* basis, and this difficulty may arise because of the strong exponential effect that temperature has on the kinetics of binder decomposition, which in turn leads to pressure within the green body. In contrast, the variational calculus algorithm [9,10] underlying the MTHC predicts the optimal balance between temperature increase, the increase in the decomposition rate constant, and the increase in the permeability of the green body as binder is decomposed. Although the MTHC is ultimately not the heating cycle which is used, the balance between the competing processes of pressure buildup and forced convection are likely preserved in the more conservative heating cycle, albeit at a lower level of threshold pressure. Or, in other words, the use of safety factors applied to the time and temperature serves to maintain the qualitative shape of the MTHC without unnecessarily prolonging it.

2.5 CONCLUSIONS

The failure behavior of multilayer green ceramic components has been determined for samples subjected to rapid thermal debinding cycles. In one case, the heating rate was held fixed for components of different size, whereas in the second case, the body size was held constant and the heating rate was varied. Under both circumstances, it was observed that failure temperature of all of the samples fell in a narrow range, and that the binder loading and maximum pressure in the center of the green body were nearly constant, independent of the size of the green body and the heating rate. The near constancy of these parameters leads to fairly consistent, relatively short, minimum time heating cycles. Safety factors can then be applied to develop more conservative debinding cycles, which however are also still fairly rapid and do not lead to component failure.

2.6 REFERENCES

1. R. M. German, "Theory of Thermal Debinding," *Int. J. Powder Metall.*, **23**, 237-245 (1987).
2. J. A. Lewis, "Binder Removal From Ceramics," *Annual Rev. Mater. Sci.*, **27**, 147-173 (1997).
3. G. Y. Stangle and I. A. Aksay, "Simultaneous Momentum, Heat and Mass Transfer With Chemical Reaction in a Disordered Porous Medium: Application to Binder Removal from a Ceramic Green Body," *Chem. Eng. Sci.,* **45**, 1719-1731 (1990).
4. D-S. Tsai, "Pressure Buildup and Internal Stresses During Binder Burnout: Numerical Analysis," *AIChE J.*, **37**, 547-554 (1991).
5. Z. C. Feng, B. He, and S. J. Lombardo, "Stress Distribution in Porous Ceramic Bodies During Binder Burnout," *J. Appl. Mech.*, **69**, 497-501 (2002).
6. S. A. Matar, M. J. Edirisinghe, J. R. G. Evans, and E. H. Twizell, "Effect of Porosity Development on the Removal of Organic Vehicle from Ceramic or Metal Moldings," *J. Mater. Res.,* **8**, 617-625 (1993).
7. J. H. Song, M. J. Edirisinghe, J. R. G. Evans, and E. H. Twizell, "Modeling the Effect of Gas Transport on the Formation of Defects during Thermolysis of Powder Moldings," *J. Mater. Res.,* **11**, 830-840 (1996).
8. Y. Shengjie, Y. C. Lam, S. C. M. Yu, and K. C. Tam, "Thermal Debinding Modeling of Mass Transport and Deformation in Powder-Injection Molding Compact," *Metall. & Mat. Trans. B-Process Metall. & Mat. Process. Sci.,* **33**, 477-488 (2002).

9. S. J. Lombardo and Z. C. Feng, "Determination of the Minimum Time for Binder Removal and Optimum Geometry for Three-Dimensional Porous Green Bodies," *J. Am. Ceram. Soc.,* **6** [12] 2087-2092 (2003).
10. S. J. Lombardo and Z. C. Feng, "Analytic Method for the Minimum Time for Binder Removal from Three-Dimensional Porous Green Bodies," *J. Mat. Res.,* **18,** 2717-2723 (2003).
11. G. Bandyopadhyay and K. W. French, "Injection-Molded Ceramics: Critical Aspects of the Binder Removal Process and Component Fabrication," *J. Europ. Ceram. Soc.* **11**, 23-34 (1993).
12. J. G. Zhang, M. J. Edirisinghe, and J. R. G. Evans, "A Catalogue of Ceramic Injection Moulding Defects and Their Causes," *Ind. Ceram.,* **9**, 72-82 (1989).
13. J. Woodthorpe, M. J. Edirisinghe, and J. R. G. Evans, "Properties of Ceramic Injection Molding Formulations. Part 3. Polymer Removal," *J. Mat. Sci.*, **24**, 1038-48 (1989).
14. J. R. G. Evans and M. J. Edirisinghe, "Interfacial Factors Affecting the Incidence of Defects in Ceramic Moldings," *J. Mat. Sci.,* **26**, 2081-2088 (1991).
15. S. A. Matar, M. J. Edirisinghe, J. R. G. Evans, E. H. Twizell, and H. Song, **"**Modelling the Removal of Organic Vehicle from Ceramic or Metal Mouldings: the Effect of Gas Permeation on the Incidence of Defects," *J. Mat. Sci., 30, 3805-3810 (1995).*
16. J. W. Yun, D. S. Krueger, P. Scheuer, and S. J. Lombardo, "Effect of Decomposition Kinetics and Failure Criteria on Binder Removal Cycles From Three-Dimensional Porous Green Bodies," *J. Am. Ceram. Soc.,* **89** [1] 176-183 (2006).
17. J. W. Yun and S. J. Lombardo, "Determination of Rapid Heating Cycles for Binder Removal from Open-Pore Green Ceramic Components," *Adv. Appl. Ceram.,* **109**, 92-101 (2009).

18. T. V. Lee and S. R. Beck, “A New Integral Approximation Formula for Kinetic Analysis of Nonisothermal TGA Data,” *AIChE J.*, **30**, 517-519 (1984).

19. S. J. Lombardo and Z. C. Feng, “Pressure Distribution during Binder Burnout in Three-Dimensional Porous Ceramic Bodies with Anisotropic Permeability,” *J. Mat. Res.,* **17**, 1434-1440 (2002).

20. J. W. Yun and S. J. Lombardo, “Methods for Introducing Safety Factors into Minimum Time Heating Cycles for Binder Removal from Green Ceramic Bodies,” *J. Ceram. Process. Res.,* **8,** 402-410 (2007)

CHAPTER 3

RELATIONSHIPS BETWEEN GREEN BODY STRENGTH, INTERNAL PRESSURE, AND STRESS DURING THERMAL DEBINDING

3.1 INTRODUCTION

During the processing of ceramic green bodies, additions of binder not only aid in the handling and subsequent processing of the green component, but the binder may also ultimately control the failure behavior during thermal debinding [1,2]. In general, the failure behavior of ceramic green bodies can be succinctly summarized by stating that failure will occur when the local stress [3-5] within the green body exceeds the local strength. The failure behavior of the green body in turns affects the duration of the debinding heating cycle. For example, when the strength of the green body is sufficiently large to withstand the stresses that accompany pressure buildup during thermal debinding, the heating cycle can be short. Conversely, if the green body is weak, the heating cycle must be correspondingly long so as to minimize pressure buildup and stress and thereby avoid failure of the green component.

In order to be able to compare the strength of a green body with the stress during binder removal, three problems must be addressed, namely: 1) the spatial distribution of pressure within the green body; 2) the spatial distribution of stress arising from the pressure field; and 3) the strength of the green body. Each of these problems in and of itself is fairly difficult to model, the reasons for which are enumerated below, but, in addition, the difficulty of each is exacerbated because the properties of the green body are changing with time and temperature during the thermal debinding heating cycle.

The first problem—the spatial distribution of pressure [3-11]—is a coupled function of the temperature distribution in the green body, the decomposition kinetics of the binder, and the permeability of the green body, all of which are changing during the heating cycle. For the case of open-pore green compacts, modeling of these coupled kinetic and transport processes

indicates that the pressure is largest at the center of the green body and decreases towards the body edges [4,5].

The second problem—the spatial distribution of stress [3-5] arising from the pressure—has also been examined, but in far fewer studies. To obtain the stress from the pressure, it is necessary to prescribe values of the material properties of the green body, and this has been generally accomplished by incorporating linear elastic behavior into mechanics models. The outcome of these studies is that the stress state within the green body consists of both normal and shear stresses, and the former are larger by approximately an order of magnitude [5]. For open-pore compacts, the largest normal stresses are found in the center of the green body, which coincides with the location of the largest pressure.

Although a common assumption, constant linear elastic behavior of the green body throughout thermal debinding is unlikely to be realistic, because both the binder loading and the mechanical properties of the green body, via the properties of the binder, are changing with time and temperature. This unrealistic assumption likely has arisen because of the absence of reported stress-strain behavior of the green body as a function of binder loading and temperature.

Two key observations from experiment, however, may partially mitigate the use of linear elastic behavior for describing the mechanical properties of the green body. First, for green bodies with high organic loadings, the stress-strain behavior is likely to be proportional, either linearly or non-linearly, up to yielding [12-18]. Beyond yielding, more complicated stress-strain behavior is possible, which likely will depend on the specifics of the binder system, the binder loading, and the ceramic particle network. If failure is assigned to the yield point, however, then only the proportionality between pressure and stress becomes important, and the use of linear elastic behavior may suffice to provide some qualitative and quantitative insight.

The second observation from experiment is that the failure temperatures of ceramic green bodies often span a relatively narrow ~30 degree C temperature range early in the heating cycle, when the binder loading is still high and nearly constant [19-21]. Thus, a description of the mechanical properties of the green body over a wide range of conditions may not necessarily be required. In light of these two observations, linear elastic behavior may again suffice, and we can thus use the results from earlier work relating pressure [11] and stress [5] in ceramic green bodies.

Finally, even if the pressure and accompanying stress state of the green body were known, little or no data have been reported on the strength of composite ceramic green bodies over a wide range of binder loading and temperature. In addition, little or no data have been presented on the elevated temperature mechanical properties of the commonly used organic constituents of the binder, either individually or in combination. This lack of data may have occurred because the binder is a fugitive species, and thus a full understanding of the mechanical properties has not been considered to be warranted. A second reason may be that because binder degradation is a kinetic process that occurs at elevated temperature, it is actually difficult to perform measurements that can be unambiguously related to the physical and mechanical state of the green body. Therefore, to describe the strength of green bodies during thermal debinding, we make recourse to simple models that capture the essential features of the mechanical behavior of composite bodies involving polymeric species, and thus use a model that incorporates the effects of time, temperature, and strain rate to predict the yield strength [12-18].

In spite of the difficulties enumerated above, it is the aim of this work to develop relationships between pressure and stress, and then to compare the stress to the strength of the composite green body as a function of temperature. We first develop a model that can then be

used to predict the strength of the green body throughout the thermal debinding cycle. We next relate the green strength during the heating cycle to the stress, which is obtained from the pressure distribution in the green body. The combination of the results from the strength, pressure, and stress models then allows us to make some qualitative assessments of how these important quantities are changing relative to each other during thermal debinding, and how they influence the observed failure behavior of green bodies during thermal debinding [19-26].

3.2 MODEL

Strength of the Green Body

To determine the strength of the green body, we start with the combined model of Rumpf [27] and Onoda [28]. The former starts with the volume fractions of solids and voids in the green body, and then ascribes the strength of the green body to forces arising at localized point contacts. Onoda [28] then modified this view by adding to the green body finite amounts of binder distributed (see Fig. 3.1) either in the pendular state or as a spherical shell coating each ceramic particle. Although the specifics of the strength of the green body depended on the amount of binder and how the binder was distributed, both the pendular- and coated-state models behaved in a similar qualitative fashion, namely, in that the green strength decreased with both decreasing fractions of ceramic and binder within the green body. For binder distributed in the pendular state, the tensile strength of a green body, σ, can be expressed as [27,28]

$$\sigma = \frac{3\sqrt{3\pi}}{8} \frac{(\varepsilon_c + \varepsilon_b)}{\sqrt{(1-\varepsilon_c-\varepsilon_b)}} \left(\frac{\varepsilon_b}{\varepsilon_c}\right)^{1/2} \sigma_b \qquad 1$$

where ε_b is the volume fraction of binder, ε is the volume fraction of pores, ε_c is the volume fraction of ceramic, and σ_b, which is the cohesive (or adhesive strength of the binder), is taken as a constant, which can be assigned to the room temperature properties of the binder.

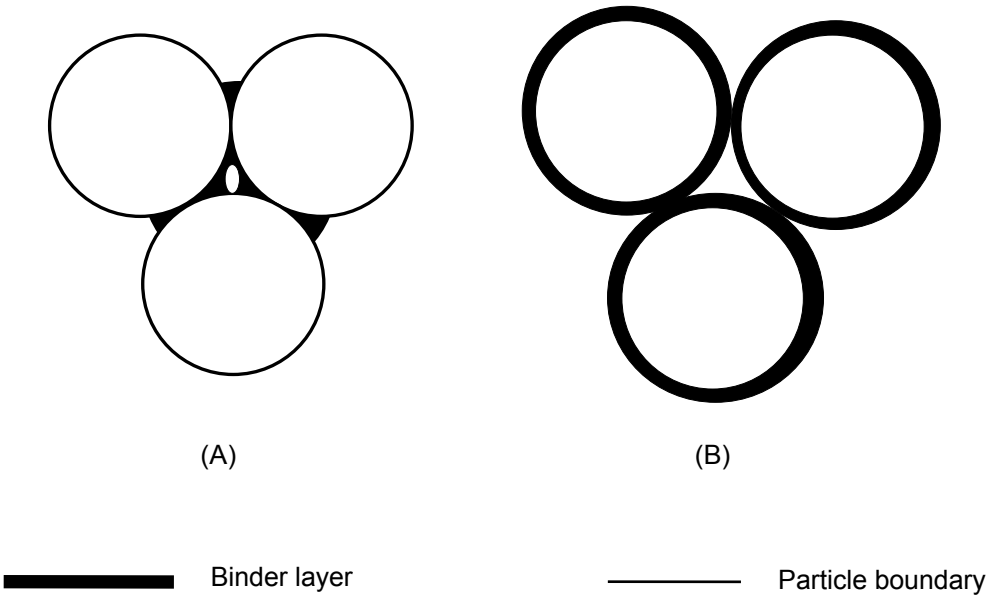

Figure 3.1 Distribution for binder between ceramic particles for (A)pendular state bonds and(B) coated state bonds

We now modify Eq. 1 because at elevated temperature, yielding of the polymeric species may occur, and it thus becomes necessary to incorporate the effects of both temperature, T, and strain rate, $\dot{\varepsilon}_y$, on the mechanical behavior of the binder. Several models are available [12-18], and for simplicity we adopt the model of Eyring [12], which is based on transition state theory. This model relates the yield strength of the polymer $\sigma_{b,y}$ to the strain rate and the activation energy, ΔH, as,

$$\sigma_{b,y} = T\left(\frac{2}{V^*}\right)\left[\frac{\Delta \mathrm{H}}{T} + 2.303R\log\left(\frac{\dot{\varepsilon}_y}{\dot{\varepsilon}_o}\right)\right] \qquad 2$$

The quantity V^* is the activation volume, $\dot{\varepsilon}_o$ is a constant, and R is the gas constant. Equation 2 can thus be used to represent the case in which yielding of polymeric or organic species occurs at elevated temperature. When Eq. 2 is used to represent the strength of the binder and is combined with Eq. 1, the strength of the green body is given by

$$\sigma = \frac{3\sqrt{3\pi}}{8}\frac{(\varepsilon_c + \varepsilon_b)}{\sqrt{(1-\varepsilon_c-\varepsilon_b)}}\left(\frac{\varepsilon_b}{\varepsilon_c}\right)^{1/2} T\left(\frac{2}{V^*}\right)\left[\frac{\Delta \mathrm{H}}{T} + 2.303R\log\left(\frac{\dot{\varepsilon}_y}{\dot{\varepsilon}_o}\right)\right] \qquad 3$$

Equation 3, which now contains the effects of both binder loading and temperature, can then be used to predict the strength of the green body throughout the thermal debinding cycle.

Internal Pressure during Binder Removal

In earlier work, we have derived in detail the coupled kinetic and transport equations for describing the internal pressure in an open-pore green ceramic body during thermal debinding. We thus here only present the relevant equations and provide references to the earlier work.

The rate of binder degradation, r, can be represented as a first order process as

$$r = -\frac{d\varepsilon_b}{dt} = A\exp\left[-\frac{E}{RT}\right]\varepsilon_b \qquad 4$$

where t is the time, A is the preexponential factor, and E is the activation energy. For a linear heating rate, β, the solution to Eq. 4 is [29]

$$\frac{\varepsilon_b}{\varepsilon_{bo}} = \exp\left[-\frac{A}{\beta}\left\{\frac{\left(\frac{RT^2}{E}\right)\exp\left(-\frac{E}{RT}\right)}{1+\frac{2RT}{E}} - \frac{\left(\frac{RT_o^{\,2}}{E}\right)\exp\left(-\frac{E}{RT_o}\right)}{1+\frac{2RT_o}{E}}\right\}\right] \qquad 5$$

where ε_{bo} is the initial volume fraction of binder and T_o is the initial temperature.

During the heating cycle for thermal debinding, the normalized pressure in the center of the green body, $(P/P_o)_o$, can be expressed as [11]

$$\left(\frac{P}{P_o}\right)_o \approx \left(1 + 0.8365\frac{\mu}{2\rho_o^2\kappa R}\frac{r\rho_b}{M}\frac{T}{T_o^2}\frac{L_x^2L_y^2L_z^2}{L_x^2L_y^2 + L_x^2L_z^2 + L_y^2L_z^2}\right)^{1/2} \qquad 6a$$

$$\approx \left(1 + G\frac{rT}{\kappa}\right)^{1/2} \qquad 6b$$

where L_x, L_y, and L_z are the dimensions of the component, μ is the gas viscosity, ρ_b is the density of the binder, M is the binder molecular weight, and ρ_o is the initial gas density in the furnace. The permeability, κ, is given by the Kozey-Carman equation as

$$\kappa = \frac{\varepsilon^3}{k(1-\varepsilon)^2 S^2} \qquad 7$$

where S is the specific surface, and k is a constant. Conservation of volume then relates the volume fractions of binder, porosity, and ceramic as

$$\varepsilon_b + \varepsilon + \varepsilon_c = 1 \qquad 8$$

Internal Stress during Binder Removal

To describe the stress within the green body [5], we use a model, derived earlier [11], for describing the internal pressure in an open-pore green ceramic body during thermal debinding. The following assumptions are further made in the development of the stress model, namely, that the porous ceramic during thermal debinding consists of a void fraction, ε, and a solid skeleton fraction, 1-ε. Secondly, the gas phase cannot support shear stresses, and both viscous and inertial stresses accompanying fluid flow are neglected. Finally, the solid skeleton is modeled as an isotropic linear-elastic solid.

Force and moment equilibrium then leads to:

$$\frac{\partial \tilde{\sigma}_{xx}}{\partial x} + \frac{\partial \tilde{\sigma}_{xy}}{\partial y} + \frac{\partial \tilde{\sigma}_{xz}}{\partial z} = \varepsilon \frac{\partial P/P_o}{\partial x} \qquad 9$$

$$\frac{\partial \tilde{\sigma}_{xy}}{\partial x} + \frac{\partial \tilde{\sigma}_{yy}}{\partial y} + \frac{\partial \tilde{\sigma}_{yz}}{\partial z} = \varepsilon \frac{\partial P/P_o}{\partial y} \qquad 10$$

$$\frac{\partial \tilde{\sigma}_{xz}}{\partial x}+\frac{\partial \tilde{\sigma}_{yz}}{\partial y}+\frac{\partial \tilde{\sigma}_{zz}}{\partial z}=\varepsilon\frac{\partial P/P_o}{\partial z} \qquad 11$$

where $\tilde{\sigma}_{ii}$ and $\tilde{\sigma}_{ij}$, (*i* and *j* correspond to *x*, *y,* and *z*) are the components of nominal normal and nominal shear stress, respectively, on the skeleton. Equations 9-11 show that an increase in internal pressure causes stress, an effect that is proportional to the void fraction. The pressure gradients on the right-hand sides are thus equivalent to a body force throughout the porous green body. The nominal stresses, $\tilde{\sigma}$, are smaller than the true stresses, σ', as given by $\tilde{\sigma}_{ij}=(1-\varepsilon)\sigma'_{ij}$. To complete the description of the problem, the skeleton is assumed to follow isotropic elastic constitutive laws with Poisson's ratio, ν=0.3, and Young's modulus, E=2×10^7 N/m^2 [4]. Equations 9-11 were solved in a commercial finite element analysis program.

3.3 RESULTS AND DISCUSSION

We first present results from Eq. 1, in which the strength of a green body depends on the volume fractions of both binder and ceramic and on the strength of the binder, which is assumed to have a constant tensile yield strength of σ_b=2.1 MPa [30] at 300 K. Figure 3.2 shows that for a given solids loading, the green strength increases strongly with binder loading. In addition, for a given binder loading, the green strength increases as the solids loading increases and this becomes more pronounced at high binder loadings as the volume fraction of solids exceeds 0.5.

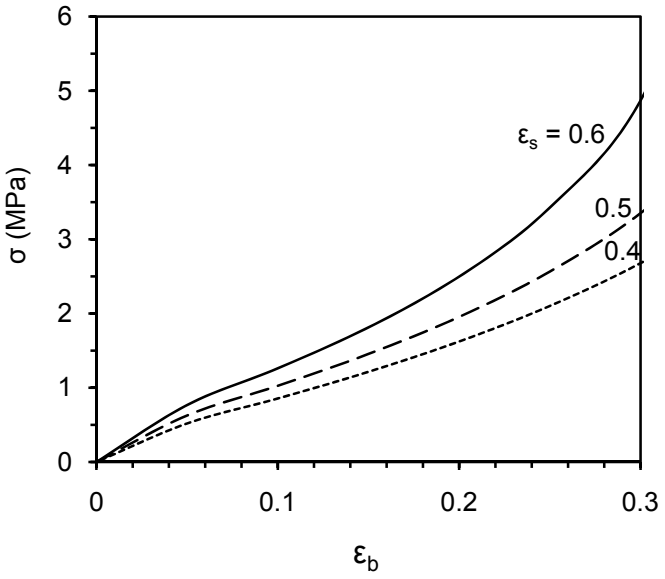

Figure 3.2: Strength (Eq. 1) versus binder volume fraction at different volume fractions of solids for pendular state bonds for σ_b=2.1 MPa.

The dependence of binder strength on temperature and strain rate as given by Eq. 2 is shown in Fig. 3.3. The yield strength decreases linearly with increasing temperature, the slope of which depends on the strain rate. For a constant temperature, decreasing the strain rate leads to a

weaker green body. In addition to the dependence on the temperature and strain rate, both the activation energy and activation volume can influence the yield strength, as seen in Fig.3.4.

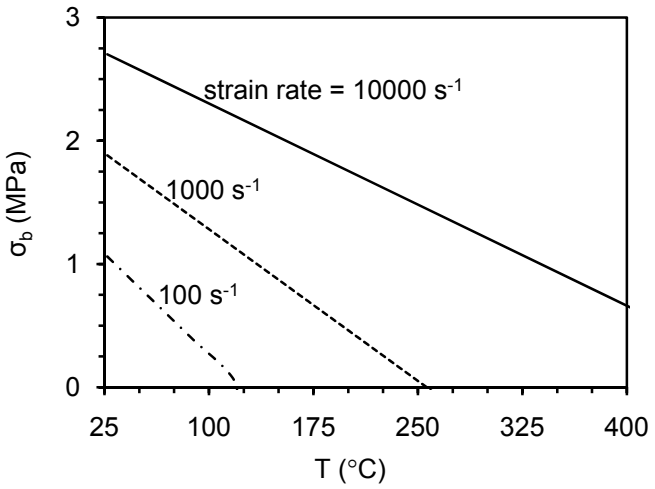

Figure 3.3: Yield strength (Eq. 2) of binder versus temperature at different strain rates with ΔH = 30.4 kJ/kmol, $\dot{\varepsilon}_o = 1\times10^6$ s^{-1}, V* =14 m^3/kmol.

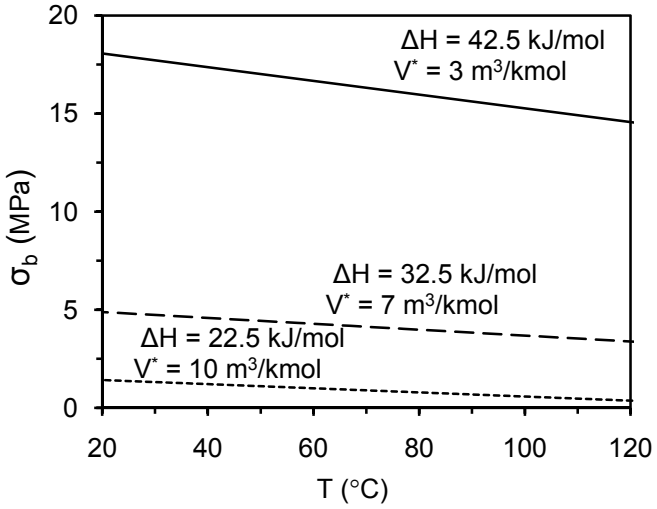

Figure 3.4: Yield strength (Eq. 2) versus temperature at constant strain rate of 1800 s^{-1} for different activation energies and activation volumes with $\dot{\varepsilon}_o = =1\times10^6$ s^{-1}.

The combined effects (Eq. 3) of binder fraction and temperature on the green strength are presented in Fig. 3.5 for a fixed ceramic loading. The green body strength increases with binder fraction and decreases with increasing temperature. Figure 3.5 also shows qualitatively a trajectory of the strength of a green body during a heating cycle from room temperature to some maximum temperature, T_{max}, followed by cooling to room temperature. For such a heating cycle, the green strength first decreases due to the degradation of binder and to the increase in temperature. Depending on where T_{max} is located in the heating cycle relative to the binder volume fraction, different behavior may arise. If T_{max} is achieved while the green body still retains binder, the strength may actually increase during the cooling branch, as is indicated by the dashed line in Fig. 3.5. For the more conventional case of binder being completely degraded on the heating branch of the cycle, then the strength of the green body decreases monotonically with decreasing volume fraction of binder. The specific strength trajectories realized during an actual debinding cycle will depend on the details of the heating cycle, which will be addressed next.

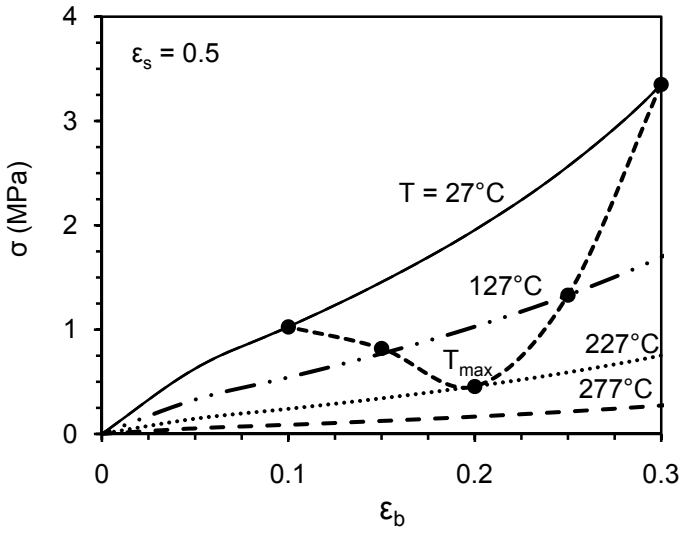

Figure 3.5: Strength (Eq. 3) versus binder volume fraction at different temperatures for a strain rate of 1800 s^{-1} ΔH = 30.4 kJ/kmol, $\dot{\varepsilon}_o$ ==1×10^6 $s^{-1}$and V^*= 14 m^3/kmol. Also shown in the figure (dashed line with arrows) is the trajectory of strength versus temperature for a heating cycle with a maximum temperature of 500 K.

To probe the failure behavior of green bodies, a simple debinding procedure can be used whereby green bodies of different sizes are fabricated and then are subjected to a rapid linear heating rate. We first show in Fig. 3.6 how the pressure in the center of the green body evolves as a function of temperature during a linear heating rate for the model parameters in Table 3.1I. The pressure first increases due to the enhanced rate of binder decomposition, then goes through a maximum, and finally decreases as binder is degraded and more void space is created in the green body. The body of larger dimensions experiences a larger internal pressure, as expected from the form of Eq. 6. Figure 3.6 also shows the evolution of the volume fraction of binder during this heating cycle, where the maximum in pressure corresponds to decomposition of

approximately 17% of the binder. For the two different sized bodies, the curves of ε_b are coincident, which can be seen from the form of Eq. 5.

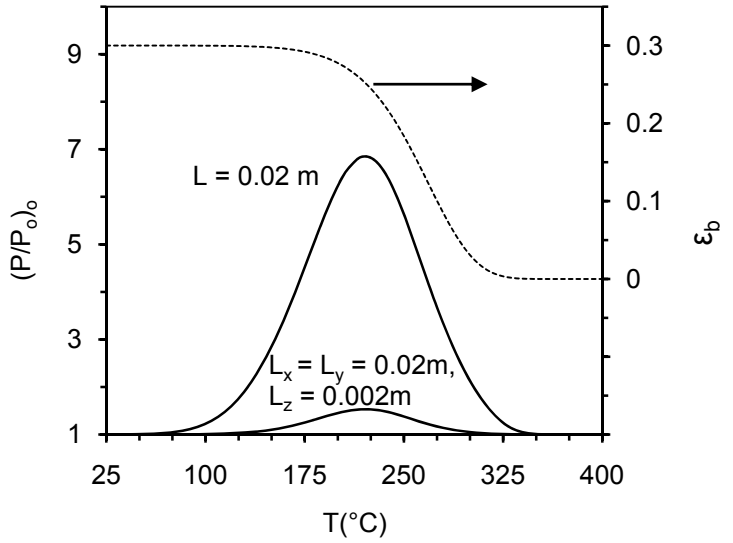

Figure 3.6: Normalized pressure in the center of the body and binder volume fraction versus temperature for a linear heating rate of 10°C/min for green bodies of two different sizes.

We can now determine from the models (Eqs. 1-3) how the strength of the green body changes during such a linear heating ramp. Curve A in Figure 3.7 shows the evolution of the green strength as given by Eq. 3, which incorporates the effects of changes in both binder loading and temperature. During the initial stage of the heating ramp, the strength of the green body decreases nearly linearly, which reflects the effect of temperature on the strength of the binder at a constant binder loading, which arises because the decomposition rate is too low. At the point in the heating cycle corresponding to the maximum in pressure, the green strength is ~25% of its initial value. Beyond the maximum in pressure, the green strength continues to decrease but now less slowly.

Table 3.1: Parameters used in the simulations.

Symbol (units)	Value
P_o (MPa)	0.1
T_o (K)	300
M (kg/mol)	0.044
R (m^3 Pa/mol K)	8.314
μ (Pa s)	2.5×10^{-5}
S (m^{-1})	6×10^{5}
k (-)	430
ρ_b (kg/m^3)	1000
ε_s (-)	0.55
ε_{bo} (-)	0.3
ε_o (-)	0.15
S (m^{-1})	6×10^{5}
k (-)	430
ρ_o (mol/m^3)	40.09
A (s^{-1})	1.7×10^{4}
E (J/mol)	68000

To see more clearly the separate effects of binder decomposition and temperature on the evolution of green strength, two additional curves are shown in Fig. 3.7. The effect of temperature alone, while holding the binder loading constant at its initial value (see Curve B), leads to a slightly more gradual decrease in strength above 175°C as compared to Curve A. If the strength of binder is taken as constant at its room temperature value (Case C), then the green body strength only depends on the volume fraction of binder, and it remains constant until appreciable binder begins to decompose. With further increases in temperature, the green strength ultimately drops to near zero in a sigmoidal fashion, which reflects the sigmoidal decrease in the volume fraction of binder with temperature (See Fig. 3.6).

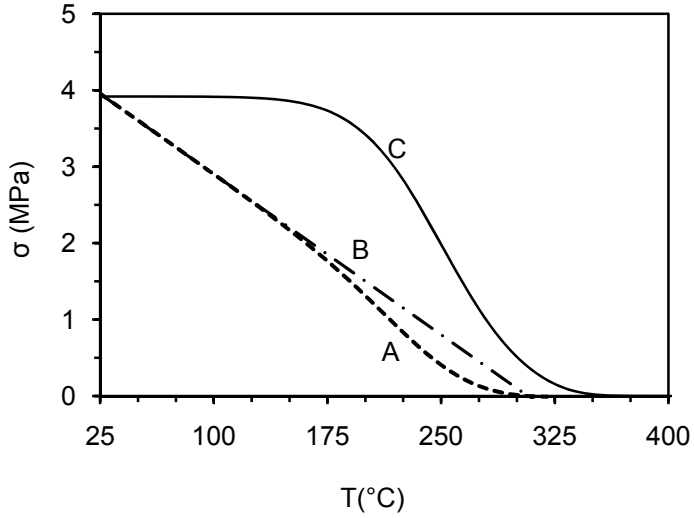

Figure 3.7: Strength (Eq. 3 with ΔH = 30.4 kJ/kmol, $\dot{\varepsilon}_o = 1\times10^6$ s^{-1}, V* =14 m^3/kmol, $\dot{\varepsilon}_y$ = =1800 s^{-1}) versus temperature for a linear heating rate for three cases: A) Both ε_b and T vary during the heating cycle; B) Varying T and $\varepsilon_b=\varepsilon\square_{b,o}$ during the heating cycle; and C) Varying ε_b and $T=T_o$ during the heating cycle.

Figures 3.6 and 3.7 can thus be used to qualitatively compare the evolution of pressure to the strength of the green body. To make a quantitative determination of failure behavior, however, the strength of the green body must be compared to the stress, which we accomplish in the following fashion. The results from Ref. [5] relate the spatial distribution of stress in ceramic green bodies as a function of the spatial distribution of pressure arising from binder decomposition. The most important outcomes of this study were that both the maximum pressure and maximum normal stress occur in the center of the green body and that the normal stresses in each direction are approximately equal and are an order of magnitude larger than the shear stresses. We thus can represent, for a cube shaped green body of 2 cm side length, the maximum normal stress, σ_{xx}, in the body center as

$$\log \sigma_{xx} \approx 0.6523 \log\left[\frac{Gr}{\alpha \kappa T}\right] + 4.72 \qquad 12$$

where

$$\alpha = \left(0.8365 \frac{1}{T_o^2}\right)^{1/2} \frac{L_y^2 L_z^2}{L_x^2 L_y^2 + L_y^2 L_z^2 + L_x^2 L_z^2} \qquad 13$$

Similar relationships are valid for green bodies of other sizes and aspect ratio.

Figure 3.8 demonstrates the evolution of normal stress in the green body versus temperature for a sample subjected to a linear heating rate. The stress profiles are now seen to mimic the pressure profiles from Fig. 3.6, which is a direct consequence of the assumptions underlying Eq. 12. Even if these assumptions are overly restrictive, however, it is still likely that during thermal debinding, the stress initially rises, reaches a maximum at some point in the heating cycle, and then ultimately decreases as the pressure in the green body decreases.

We can now superimpose the results for the evolution of the strength of the green body versus the evolution of normal stress. Figure 3.8 shows such behavior for three values of ΔH, which correspond to three room-temperature values of ε_b. In the first case, for a strong green body at room temperature, the stress in the green body never exceeds the strength, and thus the green body would survive the debinding cycle, regardless of size. For a green body of intermediate strength, the larger green body will fail near the maximum in pressure whereas the smaller green body will survive. Finally, for the weakest green body, both green bodies will fail relatively early in the heating cycle at high binder loading. This latter behavior is what was observed in Ref. [21], where green bodies of three sizes all failed early in the heating cycle over a 25 degree C temperature range.

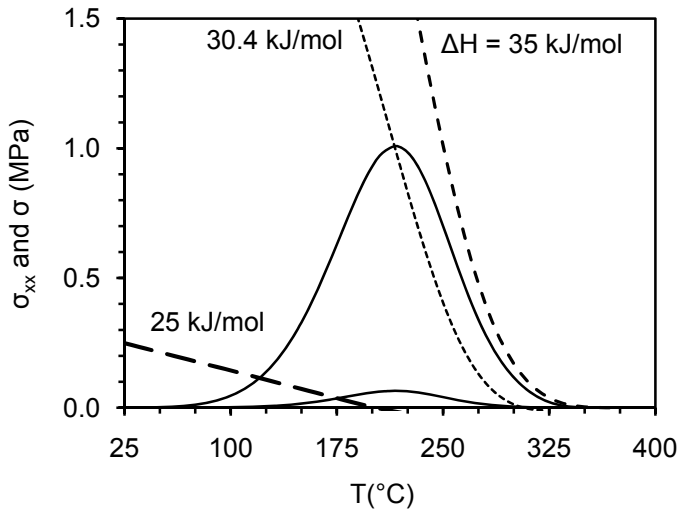

Figure 3.8: Stress in the center of the body (solid line) and green body strength (dashed line) versus temperature for a linear heating rate of 10°C/min for green bodies of two different sizes. Three cases for the strength are shown for ΔH=25 kJ/kmol, ΔH=30.4 kJ/kmol, and ΔH=35 kJ/kmol with $\dot{\varepsilon}_o = 1\times10^6$ s^{-1}, V^*=14 m^3/kmol, and $\dot{\varepsilon}_y = 1800$ s^{-1}.

A second type of procedure can be used to probe the failure behavior of green ceramic bodies during thermal debinding. In this case, bodies of constant size are subjected to heating cycles at different linear heating rates [21]. Figure 3.9 shows the profiles of pressure and volume fractions of binder during the heating cycle for this case. The pressure profiles are now shifted to higher temperatures with increasing heating rate and larger maxima in pressure occur with higher heating rates. The volume fractions of binder are also shifted to higher temperature with increasing heating rate, and they are no longer coincident, as was seen in Fig. 3.6.

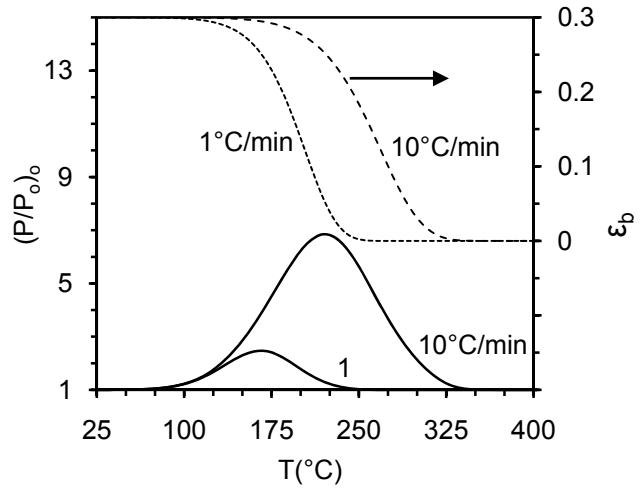

Figure 3.9: Normalized pressure in the center of the body and binder volume fraction versus temperature for a green body of fixed size at two linear heating rates.

Figure 3.10 shows the stress profiles for the same two heating rates as in Fig. 3.9. The stress profiles are also shifted to higher temperatures with larger maxima in stress occurring at higher heating rates. Comparisons of the strength of the green body and stress in the body center are also given in Fig. 3.10 for three values of ΔH, which corresponds to three room-temperature values of ε_b. Once again, the intersection of the curves—which corresponds to failure—depends on the value of the strength of the binder. For the strongest green body, the component survives, regardless of the heating rate. For the intermediate strength case, the green body will fail near the maximum in pressure for the highest heating rate, but survive for the lower heating rate. For the weakest green body, the components will fail early in the heating cycle, regardless of the heating rate. This latter case has been observed in Ref. [21].

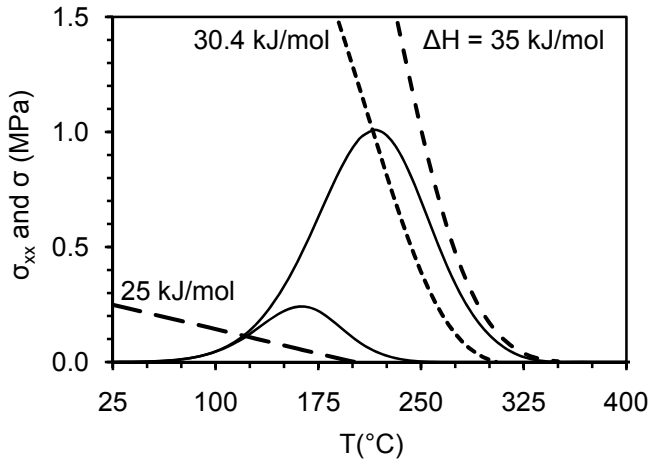

Figure 3.10: Stress in the center of the body (solid line) and green body strength (dashed line) versus temperature for a green body of fixed size at two linear heating rates (1,10). Three cases for the strength are shown for ΔH=25 kJ/kmol, ΔH=30.4 kJ/kmol, and ΔH=35 kJ/kmol with $\dot{\varepsilon}_o = 1\times10^6$ s^{-1}, V^*=14 m^3/kmol, and $\dot{\varepsilon}_y = 1800$ s^{-1}.

In summary, we have noted an absence of mechanical property data for green ceramic bodies during thermal debinding. To circumvent this shortage, we have combined different models in order to predict the strength of the green body as a function of temperature and binder loading. We have then compared the strength of the green body to the stress. This latter quantity we obtained by first incorporating the pressure distribution into a mechanics model, where we assumed linear elastic behavior. As mentioned earlier, this assumption may not be overly restrictive because up to yielding, stress and strain are likely to be proportional, and in addition, green bodies tend to fail over a narrow temperature range. In the stress model, we also did not account for the effect of temperature on the elastic modulus, which likely will impact the magnitude of the stress but may not influence the qualitative behavior of the stress reaching a maximum at some point in the heating cycle. The strength and stress profiles during thermal

debinding were then compared in order to determine their intersection, which is when failure of the green body would occur. Several of the trends for green body failure seen in Figs. 3.8 and 3.10 are consistent with what has been observed in experiments.

3.4 CONCLUSIONS

In this work, we have examined during thermal debinding how the distribution of pressure in green bodies can lead to stress, and then compared the stress to the green strength of the composite ceramic body. To make this comparison requires use of three different models for which not all of the parameters are known with high accuracy or at all. This absence of data is especially pronounced for the stress-strain behavior and strength of the green body, both as a function of temperature and binder loading. In spite of these limitations, we use simple models that likely capture the essentials of the mechanical behavior of the green body during thermal debinding. For a linear heating rate, the pressure in the center of the green body increases at low temperature as binder is decomposed and then goes through a maximum before decreasing as binder is decomposed and more porosity is created. The stress in the green body then parallels the behavior in the pressure during the heating cycle. The strength of the green body, however, is a monotonically decreasing function with both decreases in the binder loading and increases in temperature. The intersection of the stress and strength profiles then determine if and when in the heating cycle failure will occur. Several of the trends for when failure occurs are in qualitative agreement with what was observed in experiments for green body failure as a function of component size and heating rate.

3.5 REFERENCES

1. R. M. German, "Theory of Thermal Debinding," *Int. J. Powder Metall.*, **23**, 237-245 (1987).
2. J. A. Lewis, "Binder Removal from Ceramics," *Annual Rev. Mater. Sci.*, **27**, 147-173 (1997).
3. G. Y. Stangle and I. A. Aksay, "Simultaneous Momentum, Heat and Mass Transfer With Chemical Reaction in a Disordered Porous Medium: Application to Binder Removal from a Ceramic Green Body," *Chem. Eng. Sci.,* **45**, 1719-1731 (1990).
4. D-S. Tsai, "Pressure Buildup and Internal Stresses During Binder Burnout: Numerical Analysis," *AIChE J.*, **37**, 547-554 (1991).
5. Z. C. Feng, B. He, and S. J. Lombardo, "Stress Distribution in Porous Ceramic Bodies During Binder Burnout," *J. Appl. Mech.*, **69**, 497-501 (2002).
6. S. A. Matar, M. J. Edirisinghe, J. R. G. Evans, and E. H. Twizell, "Effect of Porosity Development on the Removal of Organic Vehicle from Ceramic or Metal Moldings," *J. Mater. Res.,* **8**, 617-625 (1993).
7. J. H. Song, M. J. Edirisinghe, J. R. G. Evans, and E. H. Twizell, "Modeling the Effect of Gas Transport on the Formation of Defects during Thermolysis of Powder Moldings," *J. Mater. Res.,* **11**, 830-840 (1996).
8. Y. Shengjie, Y. C. Lam, S. C. M. Yu, and K. C. Tam, "Thermal Debinding Modeling of Mass Transport and Deformation in Powder-Injection Molding Compact," *Metall. & Mat. Trans. B-Process Metall. & Mat. Process. Sci.,* **33**, 477-488 (2002).
9. S. J. Lombardo and Z. C. Feng, "Determination of the Minimum Time for Binder Removal and Optimum Geometry for Three-Dimensional Porous Green Bodies," *J. Am. Ceram. Soc.,* **6** [12] 2087-2092 (2003).

10. S. J. Lombardo and Z. C. Feng, "Analytic Method for the Minimum Time for Binder Removal from Three-Dimensional Porous Green Bodies," *J. Mat. Res.,* **18,** 2717-2723 (2003).
11. S. J. Lombardo and Z. C. Feng, "Pressure Distribution during Binder Burnout in Three-Dimensional Porous Ceramic Bodies with Anisotropic Permeability," *J. Mat. Res.,* **17**, 1434-1440 (2002).
12. T. Ree and H. Eyring, "Rheology vol. II," *Academic Press, New York*, 83–144 (1958).
13. R. N. Haward and G. Thackray, "The Use of a Mathematical Model to Describe Isothermal Stress-Strain Curves in Glassy Thermoplastics," *Proc. Roy. Soc*. *A,* **302**, 453-472 (1968).
14. D. Roylance*,* "Some Consequences of a Fracture Criterion for Oriented Polymers Based on Electron Spin Resonance Spectroscopy," *Int. J. Fracture.,* **21**, 107-114 (1983).
15. N. N. Pechanskaya and P.N. Yakushev, "Activation Parameters of Stepped Deformation of Polymers," *Phys. Solid State.,* **40**, 1486-1488 (1998).
16. J. Richeton, S. Ahzi, L. Daridon, and Y. Remond, "A Formulation of the Cooperative Model for the Yield Stress of Amorphous Polymers for a Wide Range of Strain Rate and Temperatures", *J. Polym. Sci.,* **46**, 6035-6043 (2005).
17. A. D. Mulliken and M. C. Boyce, "Mechanics of the Rate-Dependent Elastic-Plastic Deformation of Glassy Polymers from Low to High Strain Rates*," Int. J. Solids and Structures.,* **43**, 1331-1356 (2006).
18. N. G. McCrum, C. P. Buckley, and C. B. Bucknall, "Principles of Polymer Engineering," *Oxford Science Publications, New York.,* 172-174 (1997).

19. J. W. Yun, D. S. Krueger, P. Scheuer, and S. J. Lombardo, "Effect of Decomposition Kinetics and Failure Criteria on Binder Removal Cycles From Three-Dimensional Porous Green Bodies," *J. Am. Ceram. Soc.,* **89** [1] 176-183 (2006).
20. J. W. Yun and S. J. Lombardo, "Determination of Rapid Heating Cycles for Binder Removal from Open-Pore Green Ceramic Components," *Adv. Appl. Ceram.,* **109**, 92-101 (2009).
21. R. Sachanandani and S. J. Lombardo, "Effect of Green Body Size and Heating Rate on Failure During Thermal Debinding and on Debinding Cycle Time, " submitted to *J. Amer. Ceram. Soc.* (2009).
22. G. Bandyopadhyay and K. W. French, "Injection-Molded Ceramics: Critical Aspects of the Binder Removal Process and Component Fabrication," *J. Europ. Ceram. Soc.* **11**, 23-34 (1993).
23. J. G. Zhang, M. J. Edirisinghe, and J. R. G. Evans, "A Catalogue of Ceramic Injection Moulding Defects and Their Causes," *Ind. Ceram.,* **9**, 72-82 (1989).
24. J. Woodthorpe, M. J. Edirisinghe, and J. R. G. Evans, "Properties of Ceramic Injection Molding Formulations. Part 3. Polymer Removal," *J. Mat. Sci.*, **24**, 1038-1048 (1989).
25. J. R. G. Evans and M. J. Edirisinghe, "Interfacial Factors Affecting the Incidence of Defects in Ceramic Moldings," *J. Mat. Sci.,* **26**, 2081-2088 (1991).
26. S. A. Matar, M. J. Edirisinghe, J. R. G. Evans, E. H. Twizell, and H. Song, "Modelling the Removal of Organic Vehicle from Ceramic or Metal Mouldings: the Effect of Gas Permeation on the Incidence of Defects," *J. Mat. Sci.,* **30**, 3805-3810 (1995).
27. H. Rumpf, *The Strength of Granules and Agglomerates: International Symposium on Agglomeration*, Interscience, London, UK, 1962.

28. G. Onoda, “Theoretical Strength of Dried Green Bodies with Organic Binders,” *J. Am. Ceram. Soc.,* **59** [5] 236-239 (1976).

29. T. V. Lee and S. R. Beck, “A New Integral Approximation Formula for Kinetic Analysis of Nonisothermal TGA Data,” *AIChE J.*, **30**, 517-519 (1984).

30. R. Sachanandani, “ Failure Analysis of Green Ceramic bodies During Thermal Debinding” M.S.Thesis,(2009).

CHAPTER 4

TENSILE PROPERTIES OF GREEN CERAMIC TAPES AND BINDER TAPES

4.1 INTRODUCTION

Green body formation is an important step in the fabrication of ceramic capacitors, as it influences the properties of the final product. Binders (polymers) are often added to provide sufficient strength, so that the green body can survive the subsequent stages of ceramic processing [1-3]. Prior to the sintering stage, the removal of binder by thermal decomposition can lead to failure of the green body. Failure may be due to insufficient green strength or may be due to high stresses arising from the binder removal process [4]. Therefore, it is essential to have some insight of the mechanical properties of the green body which can eventually be used to assist in developing optimum binder removal cycles.

As proposed by Onoda [5,6], the strength of green body depends on the binder content and the mechanical strength of the binder system. The strength of the binder can be represented as the cohesive strength of the binder or the adhesive strength at the binder-ceramic interface. As discussed in Chapter 3, the failure behavior effects the duration of the binder removal heating cycle, it becomes essential to have knowledge of the mechanical properties of the green ceramic bodies at different binder loadings and temperature. In this work, we have studied the tensile properties of the green tapes at various binder loadings and the binder system which is composed of binder, plasticizer and other organic additives.

4.2 EXPERIMENTAL

Green ceramic tapes were prepared from barium titanate powder (Tamtron X7R 422H, Ferro Electronic Materials, Niagara Falls, NY), which has a mean particle diameter of 1.1 □m and specific surface area of 3.0 m^2/g. A slurry was prepared at 65 weight% powder with 35 weight% binder solution consisting of 14.5 weight% poly(vinyl butyral) binder (Butvar B98, Richard E. Mistler, Inc., Yardley PA), 10.9% butyl benzyl phthalate plasticizer (Santicizer 160, Richard E. Mistler, Inc.) and 3.8% blown Menhaden fish oil (Z-3, Richard E. Mistler, Inc.) in a mixture of 35.4% each of xylene and ethanol. After ball milling, the slurry was de-aired and then filtered through a 53 μm nylon mesh. The slurry was then tape cast with a single stationary doctor blade on a Mylar carrier film. After drying, the thickness of the tapes was approximately 150-160 μm. Then tapes were then placed in an oven at 185^{o}C and were removed from the oven at different times to decrease the binder content which was originally 10.8% by weight. The tapes were cut in accordance with the ASTM method [7]. The dimensions of the sample were determined, which was placed in the tensile tester. The tensile strength was then measured using tensile tester (TA HD*i* Texture Analyzer, Stable Micro Systems Ltd. Surrey, UK) with data being recorded as force in Newtons versus distance and time (s). Samples with different binder loadings conditions were subjected to an extension rate of 0.5 mm/s. Due to the fragility of green tapes at lower binder loadings, it was only feasible to make measurements at greater than 80% of binder present originally.

To study the tensile properties of the binder system itself, thin tapes composed of poly(vinyl butyral) (44.4%) binder (Butvar B98, Richard E. Mistler, Inc., Yardley PA), butyl benzyl phthalate plasticizer (44.4%) (Santicizer 160, Richard E. Mistler, Inc.) and blown Menhaden fish oil (11.2%) (Z-3, Richard E. Mistler, Inc), were prepared by tape casting to a

thickness of 130-150 μm and allowed to dry for ~10 h. These tapes were tested and the tensile properties were determined with the approach described above.

The engineering strain ε

. at any instant is given by,

$$\varepsilon = \frac{l_i - l_o}{l_o} = \frac{\Delta l}{l_o} \qquad 1$$

where l_o is initial gauge length, and l_i is the instantaneous gauge length. The engineering stress σ, can be calculated as:

$$\sigma = \frac{F}{A_o} \qquad 2$$

where F is the applied force and A_0 is the original cross-sectional area.

To have an understanding of materials with appreciable elasticity it is essential to determine the true stress-strain behavior. To evaluate the true stress σ_t, and true strain ε_t, the approximation of constant volume is made, wherein the deformation of the green body is assumed reversible, which leads to the following relations [8]:

$$\varepsilon_t = \ln\left(\frac{l_i}{l_o}\right) = \ln(1+\varepsilon) \qquad 3$$

$$\sigma_t = \frac{F}{A_i} = \sigma(1+\varepsilon) \qquad 4$$

where A_i is the instantaneous cross-sectional area which decreases as force is applied.

4.3 RESULTS AND DISCUSSION

Green ceramic tapes with 0%, 8%, 12.5% and 18.5 % binder removed, were subjected to tensile loading. Figure 4.1 shows the green tape images for before and after testing. For green tapes with identical binder content, the failure occurred at different locations along the length of the tape, indicating sample to sample variation. It was seen that subsequent to failure, the dimensions of the sample remained unchanged which is indicative of the fact that failure occurred in the elastic region and plasticity was not reached. This type of behavior is typical for ceramic materials as they typically do not exhibit appreciable plastic deformation.

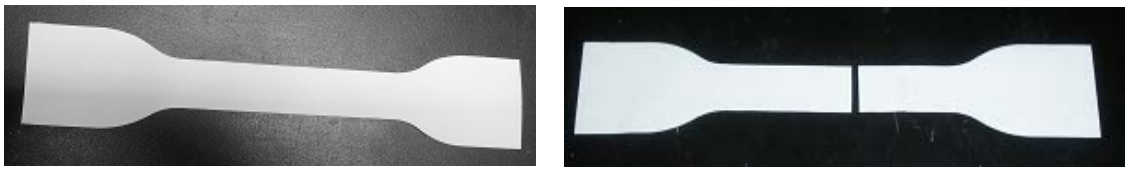

Figure 4.1: Images of green ceramic tape for no binder removed, before and after tensile testing. Failure occurred at the centre of the sample.

Engineering stress-strain data which were obtained, were eventually converted to true stress-strain data. Figure 4.2 shows both engineering and true stress-strain data for three green tapes, with no binder removed. The engineering stress and the true stress at failure differed by ~25% whereas the strains differed by ~10%. The magnitude of true stress and true strain at failure varied from 2.1-3.1 MPa and 22-35% respectively. As expected, the true stress was greater than the engineering stress but the true strain was less compared to the engineering strain, owing to the assumption of constant volume during deformation.

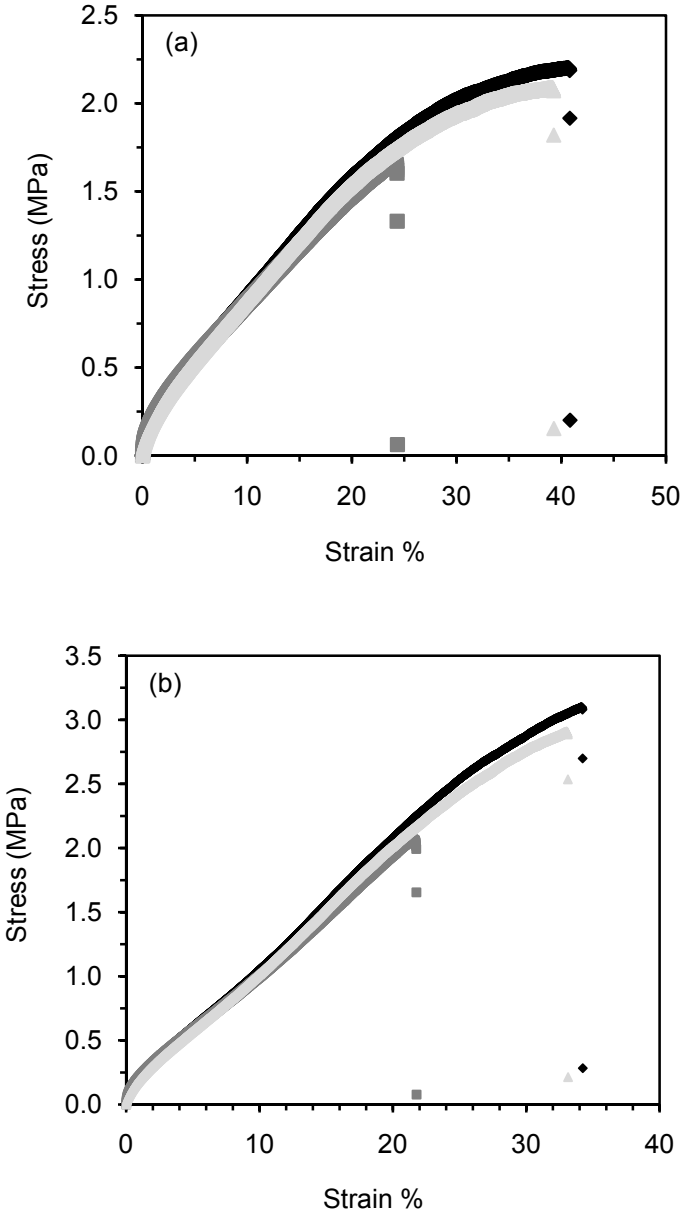

Figure 4.2: (a) Engineering stress-strain data (b) True stress-strain data for green tapes with no binder removed.

In Figure 4.3 which describes the stress-strain behavior for 8% binder removed, the magnitude of true stress and true strain at failure varied from 1.9-3 MPa and 14-26% respectively. Green tapes with binder removed condition exhibit brittle behavior. For tapes with 12.5% binder removed the stress-strain data is shown in figure 4.4. The magnitude of true stress and true strain at failure varied from 2.2-3.2 MPa and 9-19% respectively. Differences were observed in the Engineering stress-strain data and the true stress-strain data.

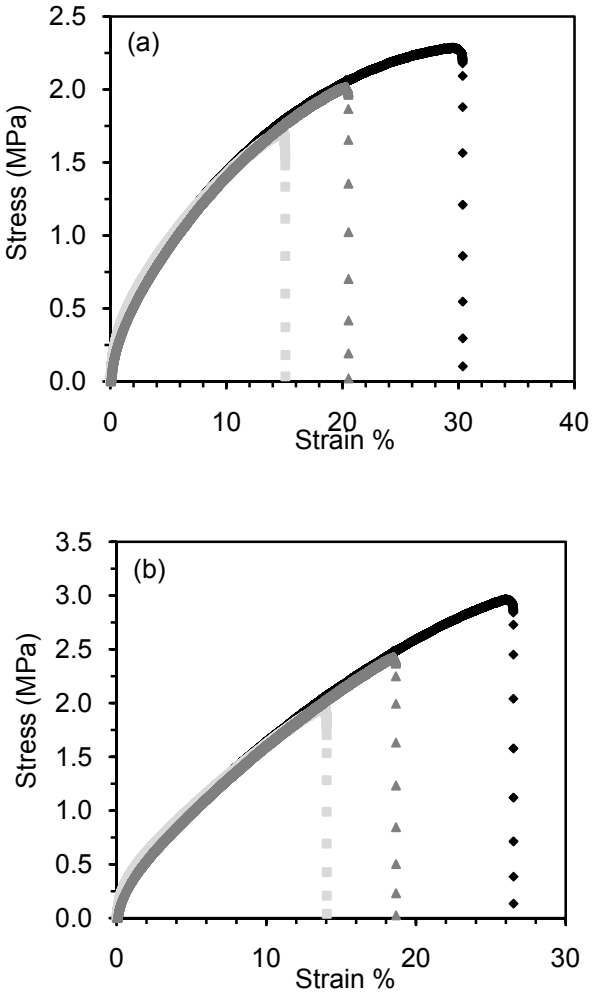

Figure 4.3: (a) Engineering stress-strain data (b) True stress-strain data for green tapes with 8% binder removed.

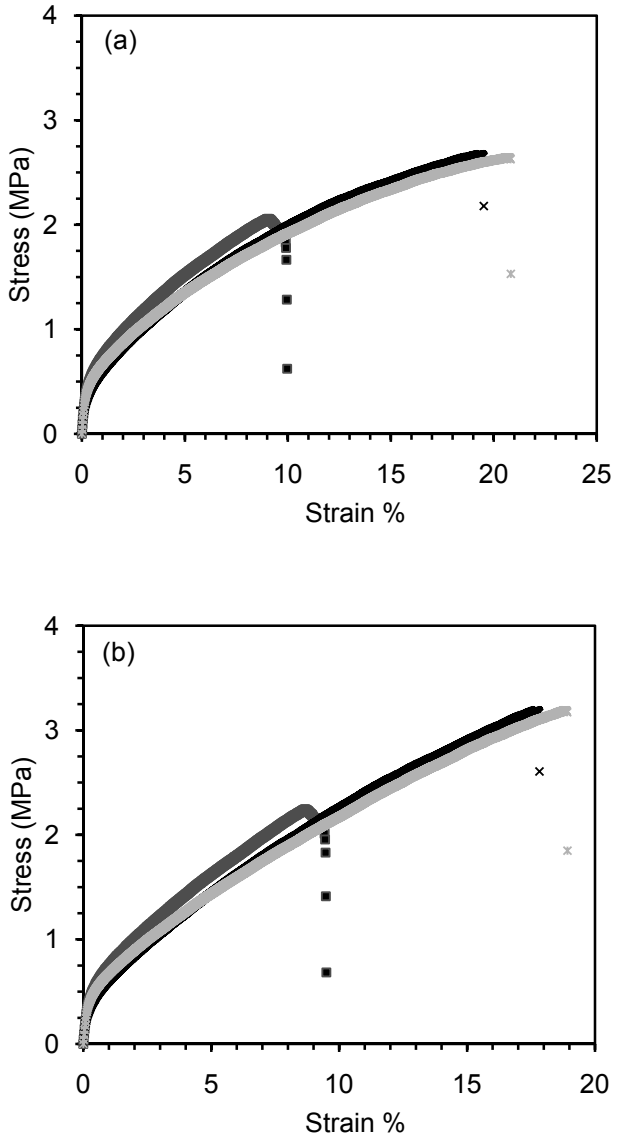

Figure 4.4: (a) Engineering stress-strain data (b) True stress-strain data for green tapes with 12.5% binder removed.

The stress-strain behavior for 18.5% binder removed condition is shown in figure 4.5. The magnitude of true stress and true strain at failure varied from 2.1-2.5 MPa and 6-10% respectively. For the different cases of binder content, a significant change in the tensile strength

is not seen which could be due to the fact that as we are analyzing tapes at a maximum~20% of the original binder content, the green tapes would contain the Poly vinyl butyral (PVB) which is the green strength providing binder ingredient and thus the organic loss may be of the plasticizer which is butyl benzyl phthalate in our case. Plasticizer provides flexibility to the green tape which can be seen for the no binder lost tapes, where the failure occurs at higher strains when compared to tapes with lower binder content. Also, plasticizer contributes appreciably in the binder composition which is about 44.4%.

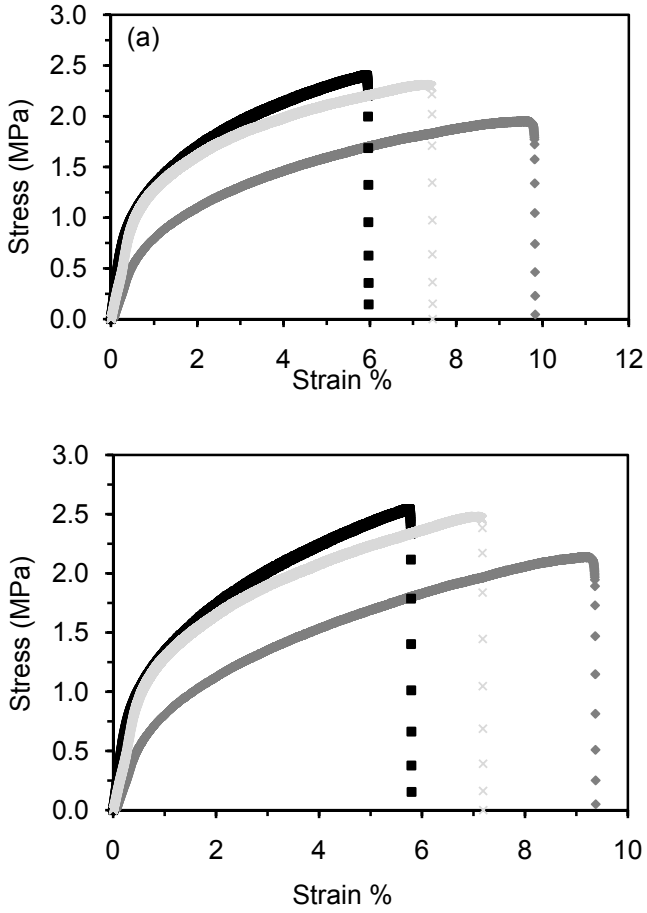

Figure 4.5: (a) Engineering stress-strain data (b) True stress-strain data for green tapes with 18.5% binder removed

The average true stress, true strain at failure and modulus of elasticity data for the different binder loadings are summarized in Table 4.1. For this small range of binder loadings, the green tapes did not show significant change in the tensile strength whereas the strain at failure varied from 7-29% showing, describing the brittleness of the samples. The modulus of elasticity was determined at strain of 0.5 %. For evaluating modulus of elasticity secant modulus was used which represents the slope of a secant drawn from the origin to some given point on the stress-strain curve. The modulus of elasticity increases as the binder is removed, which is due to increase in slope of the stress-strain plot as the binder is removed.

Table 4.1: Summary of true stress, true strain at failure and elastic modulus for green tapes with different binder loadings.

% binder lost	Strain % at failure	Stress at failure (MPa)	Modulus of Elasticity (MPa)
0	28.7 ± 6.9	2.8 ± 0.75	28.1 ± 3.3
8	18.8 ± 6.2	2.4 ± 0.50	51.6 ± 6.5
12.5	14.8 ± 5.5	2.8 ± 0.54	103.6 ± 12.7
18.5	7.2 ± 1.8	2.3 ± 0.21	164.7 ± 51.6

Figure 4.6 shows the variation in true strain at failure with decreasing binder content. The strain changes significantly with loss of ~20% of the original binder content. The true stress at failure does not change appreciably and is nearly constant within this span of binder loading, but the sample variation at each binder loading shows a decreasing trend which is indicated by decrease in standard deviation.

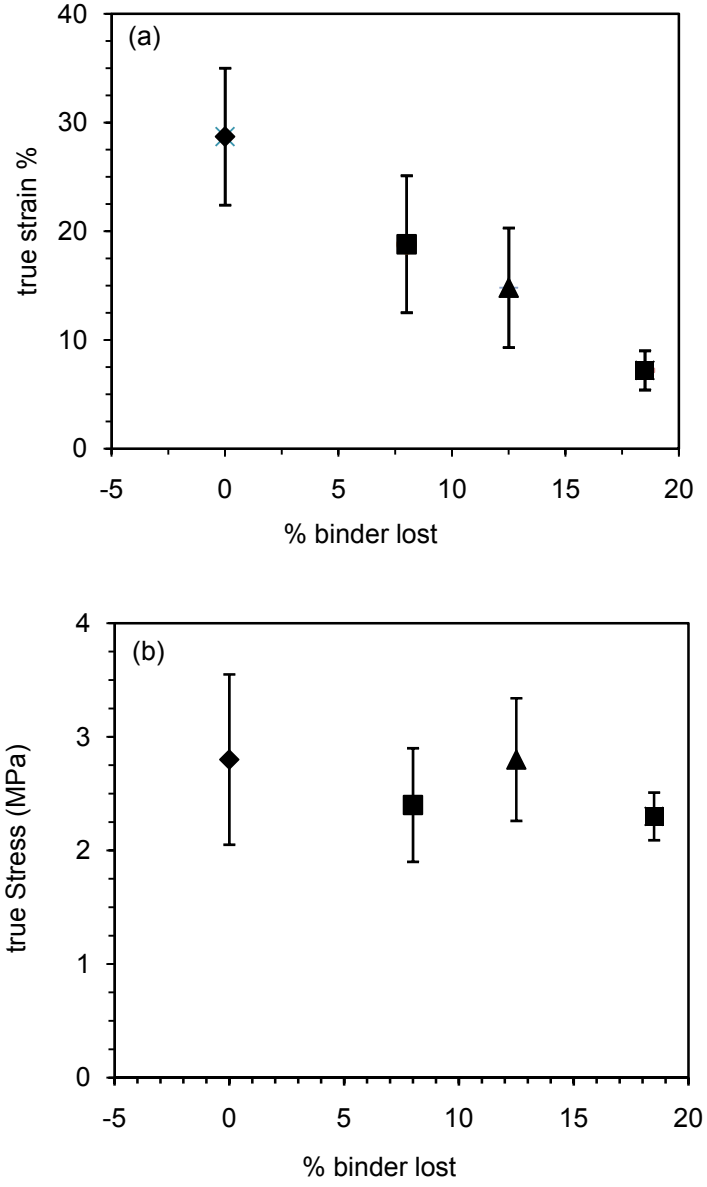

Figure 4.6: (a) True strain at failure versus % binder lost and (b) true stress at failure versus % binder lost for green ceramic tapes.

Binder tapes comprised of the binder (polyvinyl butyral) and plasticizer (butyl benzyl phthalate) were also tested and true stress-strain data were determined. As observed in figure 4.7, the engineering stress at failure was ~0.7 MPa and engineering strain was 200-250%, whereas

the true stress at failure was in the range of 2-2.5 MPa and true strain at failure from 110-130%. The binder tapes showed enormous flexibility, indicated by high strains. As mentioned earlier, the flexibility seen in the green tapes is provided by the plasticizer whereas the green strength is provided mainly by the binder, with possibly some mechanical interlocking provided by the particle network. Such behavior is qualitatively consistent with the strength model given by equation 1 in Chapter 3.

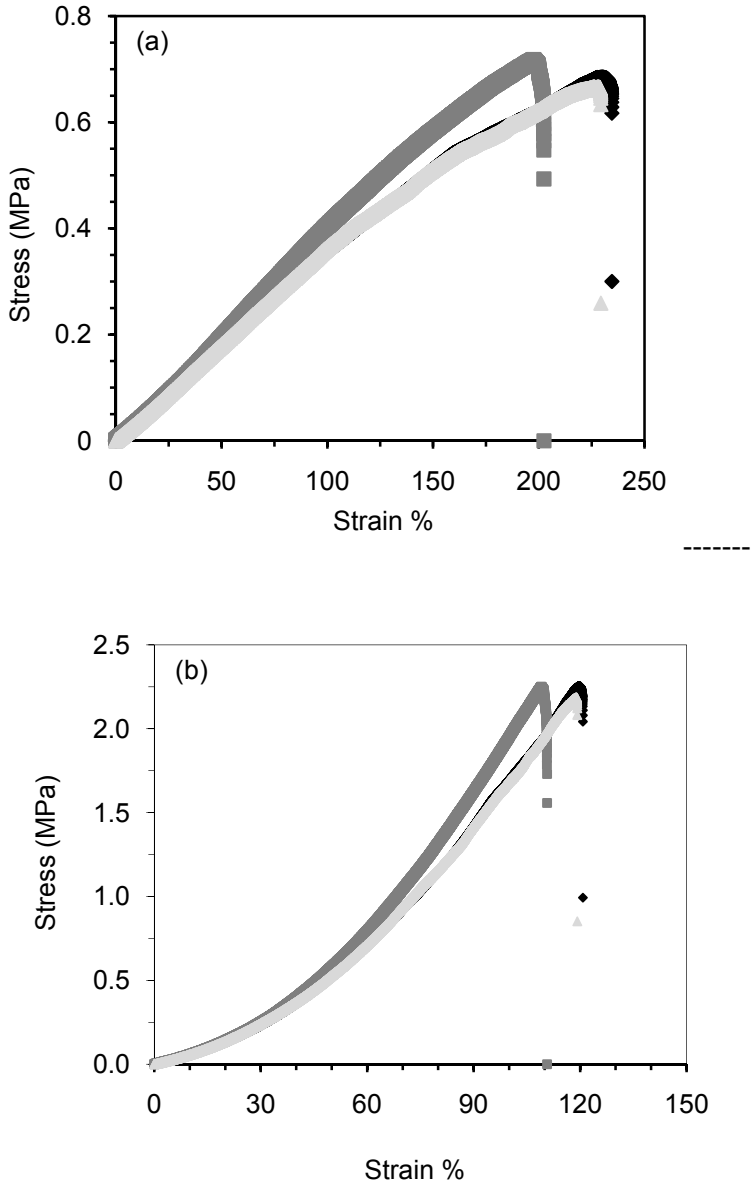

Figure 4.7: (a) Engineering stress versus strain and (b) True stress versus strain for binder film mainly consisting of the poly vinyl butyral and butyl benzyl phthalate.

4.4 CONCLUSION

The tensile properties for the green ceramic tapes and binder tapes have been determined at room temperature. For the green ceramic tapes, tensile properties at different binder loading are presented. The tensile strength for the given range of binder loading did not show significant change. The strain at failure decreased significantly, due to the loss of plasticizer. The tensile properties of binder tapes comprising mainly of the binder (poly vinyl butyral) and the plasticizer (butyl benzyl phthalate) displayed flexibility with larger strains at failure.

4.5 REFERENCES

1. J. A. Lewis, "Binder Removal From Ceramics," *Annual Rev. Mater. Sci.*, **27**, 147-173 (1997).
2. G. Bandyopadhyay and K. W. French, "Injection-Molded Ceramics: Critical Aspects of the Binder Removal Process and Component Fabrication," *J. Europ. Ceram. Soc.* **11**, 23-34 (1993).
3. R. M. German, "Theory of Thermal Debinding," *Int. J. Powder Metall.*, **23**, 237-245 (1987).
4. J. W. Yun, D. S. Krueger, P. Scheuer, and S. J. Lombardo, "Effect of Decomposition Kinetics and Failure Criteria on Binder Removal Cycles From Three-Dimensional Porous Green Bodies," *J. Am. Ceram. Soc.,* **89** [1] 176-183 (2006).
5. H. Rumpf, "The Strength of Granules and Agglomerates: International Symposium on Agglomeration", Interscience, London, UK, 1962.
6. G. Onoda, "Theoretical Strength of Dried Green Bodies with Organic Binders," *J. Am. Ceram. Soc.,* **59** [5] 236-239 (1976).
7. "Standard Test Method for Tensile Properties of Plastics", ASTM designation: D 638-03 approved (2003)
8. H. Czichos, T. Saito, L. Smith (Eds.), "Springer Handbook of Materials Measurement Methods", Springer Publication (2006)

CHAPTER 5

CONCLUSIONS AND FUTURE WORK

5.1 CONCLUSIONS

The failure behavior of multilayer green ceramic components has been determined by subjecting the green body to rapid binder removal heating cycles for the following cases (a) the heating rate fixed with varied component dimensions, and (b) component size constant with various heating rates. For both the cases, the failure temperature showed dependency on the heating rate and body size. The binder loading at failure and maximum pressure in the center of the green body, however, were nearly constant. The minimum time heating cycles (MTHC), determined using these failure conditions, were very short in duration. Safety factors were then used to develop more conservative debinding cycles.

The pressure distribution in the green bodies was used to describe the stress distribution and the stress was then compared to the green strength of the composite ceramic body during thermal debinding. To make this comparison, three models were used for which not all the parameters were known with high accuracy. The stress distribution throughout the binder removal cycle was parallel to the pressure distribution, whereas the strength of the green body decreased monotonically both as a function of binder content and temperature. The intersection of the stress and strength profiles was used to determine if and when in the heating cycle failure will occur. In spite of the limitations, simple models were used to capture the essentials of the mechanical behavior of the green body during the binder removal heating cycle. Additionally, the tensile properties of the green tapes at different binder loadings and binder tapes alone were experimentally determined.

5.2 FUTURE WORK

Knowledge of the failure behavior of a green body during binder removal is very important, because information of failure behavior would assist in developing more rapid thermal debinding cycles. A step forward in understanding the failure behavior would be to identify the mechanism (tension, adhesion, shear, compression etc) which causes failure.

With inadequate information available in the literature for the mechanical properties of binder systems and green bodies, it is essential to study the mechanical properties of binders and green bodies at different binder loadings and at elevated temperatures and use this in the model to have a clear idea of the green body strength.

Finally, to describe the strength of green body, we have solely taken into account the yielding behavior of binders. Other aspects like binder-ceramic particle interactions and binder-binder interactions must also be studied and considered in the strength model.

APPENDIX

DETERMINATION OF POROSITY, GAS PERMEABILITY, AND BINDER DECOMPOSITION KINETICS

A.1 EXPERIMENTAL

Five green tapes cut into disks of 2.5 cm diameter were stacked and laminated in a press at 7 MPa and 85°C for 10 min. Three samples were made using the above procedure. To determine the void volume, ε of the laminated tapes, the water uptake at room temperature in the pores of the sample was determined as a function of time. The porosity is then related to the volume fractions of the solid, ε_c and binder, ε_b, as [1]

$$\varepsilon = 1 - \varepsilon_c - \varepsilon_b \qquad 1$$

To perform the permeability measurements, laminated green tapes of disk geometry were inserted into a sample holder with an open area of 1.56 cm in diameter and sealed with a flexible o-ring. An upstream pressure of nitrogen was set by a pressure regulator, and the downstream pressure could be adjusted by the valve before the flow meter. The volumetric flow rate, V_f, in the flow meter was monitored and then converted to a molar flow rate, n, via

$$n = \frac{P_f V_f}{R T_f} \qquad 2$$

where P is the pressure, R is the gas constant, T is the temperature, M is the molecular weight of the gas, and the subscript f denotes the conditions at the flow meter. The molar flux, N, through the area, A, of the substrate is then given by

$$N = \frac{m}{A} = u_o \rho \qquad 3$$

where u_o is the superficial velocity and ρ is the molar density. The flux given by Eq. 3 is a quantity determined solely by experiment and contains no microstructural features of the porous green body.

To determine the kinetics of binder degradation [2,3], weight loss experiments were conducted in flowing air with a thermogravimetric analyzer at heating rates of β = 1 and 10 °C/min. To determine values for the pre-exponential factor *A,* and the activation energy *E,* from the weight loss data, we assume or establish a decomposition mechanism as a function of binder concentration and then use an integral form of the kinetic expression. For a general kinetic process, $f(\alpha)$, where α=1-$\varepsilon_b/\varepsilon_{b,o}$ is the fraction of reacted binder, the rate expression for a thermally activated process can be represented as

$$\frac{d\alpha}{dt} = A\exp\left[\frac{-E}{RT}\right]f(\alpha) \qquad 4$$

For TGA experiments conducted with a constant heating rate, β, *A,* and *E* can be determined from:

$$\ln\left[\frac{F(\alpha)}{T^2}\right] = \ln\left[\frac{AR}{\beta(E+2RT)}\right] - \frac{E}{RT} \qquad 5$$

where $F(\alpha)$ is the integrated form of $f(\alpha)$. Many forms of $f(\alpha)$ and hence $F(\alpha)$ have been proposed. Here, we examine first-order kinetics, for which $f(\alpha)=(1-\alpha)$ and $F(\alpha)=-ln(1-\alpha)$.

A.2 RESULTS

The porosity of the laminated tapes was measured by submerging the samples in water at 21°C until the curves of water uptake reached a plateau; the water uptake was then converted to porosity. Figure A.1 shows that after ~90 h, plateaus in the porosity versus time have been reached. The porosity ranged from 0.12-0.15, which indicates some sample to sample variation which may be because of certain degree of inaccuracy in lamination of the samples. Porosity value of 0.15 is used in the simulations in Chapters 2 and 3.

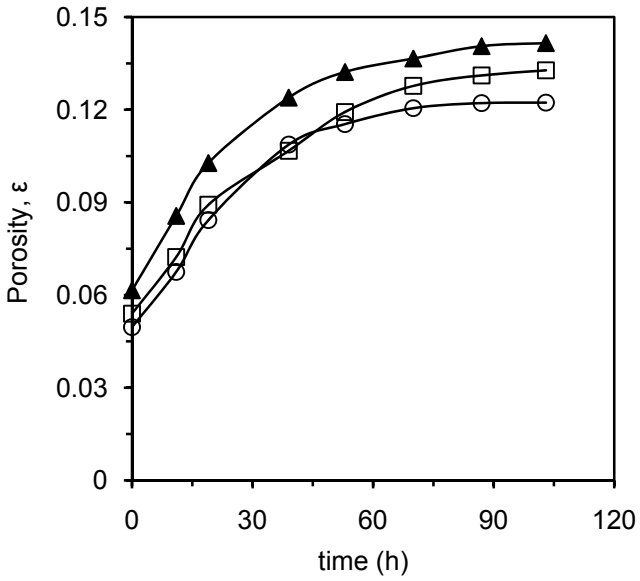

Figure A.1: Porosity of laminated tapes measured at atmospheric conditions as a function of time. Each sample contains 5 green tapes laminated at 7 MPa and 85^{o}C for 10 min.

To determine the characteristic pore size which governs the observed flow behavior, we used the procedure proposed in Refs.[4,5], whereby we obtain the flux as a function of the arithmetic mean pressure, P_{ave}. At higher pressures, where Knudsen flow can be neglected, a plot of the normalized flux versus mean pressure yields a linear relation

$$\frac{N}{\Delta P} = AP_{ave} + B \quad (6)$$

where A is the slope and B is the intercept. The ratio of

$$\frac{A}{B} = \frac{3\bar{r}}{4\pi\mu\bar{v}} \quad (7)$$

can then be used to determine the characteristic pore diameter, $D = 2\bar{r}$, where μ is the viscosity of the gas. The quantity $\bar{v} = (8RT/\pi M)^{1/2}$ is the average velocity in terms of the molecular weight of the gas-phase species. The characteristic pore size can then be used to determine the specific surface, *S*, in terms of an equivalent pore diameter as

$$S = \frac{4\varepsilon}{(1-\varepsilon)D} \quad (8)$$

If the pore size is sufficiently large, then Poiseuille flow is the dominant transport mechanism and the permeability can be calculated using Darcy's Law [6]:

$$\kappa = -2RTN\mu\frac{L}{P_2^2 - P_1^2} \quad (9)$$

The permeability in Eq. 9, which is based solely on flux measurements, can then be expressed in terms of microstructural attributes of the green body by the Kozeny-Carmen equation as [4]

$$\kappa = \frac{\varepsilon^3}{k(1-\varepsilon)^2 S^2} \quad (10)$$

where *k* is the parameter to account for tortuosity and constrictions in the pore space.

The pore size was determined for 3 laminated samples by plotting $N/\Delta P$, versus P_{ave}. As seen in figure A.2, the plots bear an approximate linear relationship. Some variation is evident in the normalized flux plots, which may be due to sample to sample variation and inaccuracy in measurement.

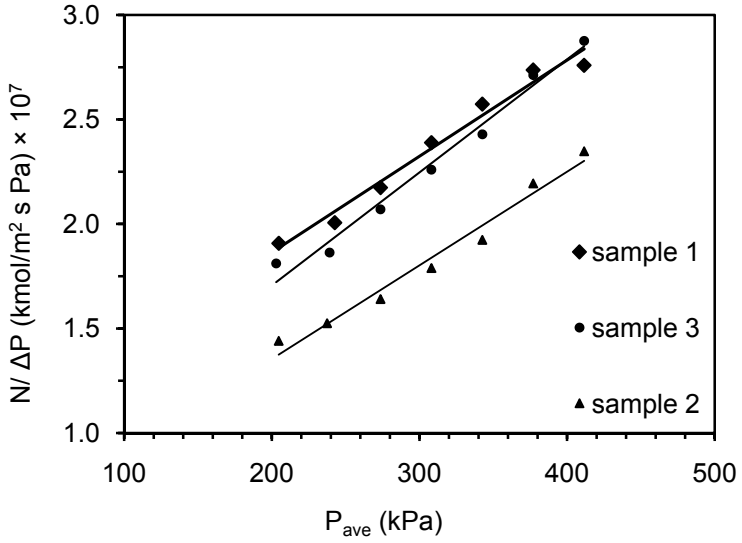

Figure A.2: Normalized flux versus average pressure for laminated tapes. Each sample contains five green tapes laminated at 7 MPa and 85^{o}C for 10 min.

The summary of permeability, pore size, specific surface and tortuosity is listed in table A.1. The average permeability values for the laminated tapes was nearly constant, whereas the pore diameter, specific surface and tortuosity showed significant variation.The average values of these parameters is used in the simulations in Chapters 2 and 3.

Table A.1: Summary of permeability, hydraulic diameter, specific surface, porosity, and parameter for tortuosity for three samples which consists of five green tapes laminated at 85°C and 7 MPa for 10 min.

Sample	Permeability range $\kappa \times 10^{17}(m^2)$	Hydraulic pore Diameter $4\times r$ (μm)	Specific Surface $S\ (m^{-1})$	Porosity ε	tortuosity k
Sample 1	2.5-3.5 $\kappa_{avg} = 2.92$	0.695	8.59×10^5	0.117	134.7
Sample 2	2.1-2.6 $\kappa_{avg} = 2.26$	1.384	4.03×10^5	0.122	677.9
Sample 3	2.6-3.3 $\kappa_{avg} = 2.81$	1.227	5.48×10^5 $S_{avg}= 6\times10^5$	0.143	480.6 $k_{avg}= 430$

The weight loss of binder from a green body as a function of temperature is displayed in Figure A.3 for heating rates of 1and 10 °C/min and the total weight loss was 10.8%. The TGA data was then analyzed using equation 5. As can be seen in figure A.3, there are two regions rapid of binder decomposition and the predicted mechanism of first order kinetics describes the weight loss in the first region of decomposition. It is also seen in Chapter 2, the failure of green bodies occur at high binder loadings. The predicted E = 68 kJ/mol and $A = 1.70\times10^4\ s^{-1}$ for β = 10 °C/min describe the TGA data for (1-α) = 0.99-0.66. The above values are then used in the simulations in Chapter 2 and 3.

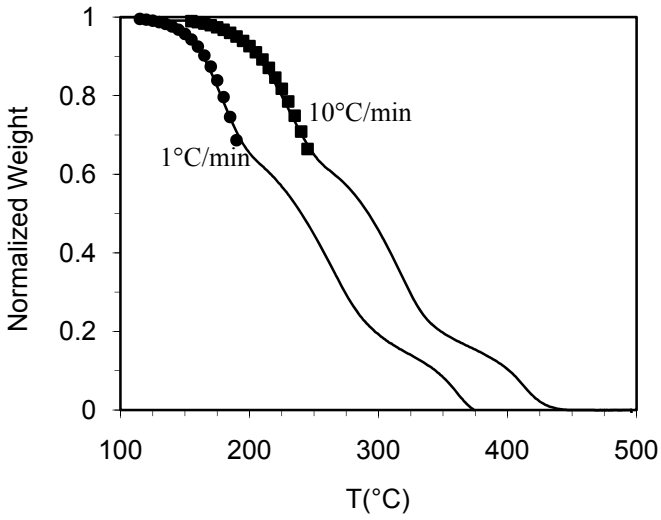

Figure A.3: Thermogravimetric analyzer weight loss data in air for polyvinyl butyral and butyl benzyl phthalate binder system in presence of barium titanate at different linear heating rates. The predicted kinetics with the first order mechanism are indicated by symbols.

A.3 CONCLUSIONS

The porosity of the laminated tapes was measured at room temperature which showed some sample variation. The permeability of the laminated green ceramic tapes was determined and eventually used to evaluate the specific surface, tortuosity and characteristic pore size. The kinetics of the binder decomposition was predicted for the first region of decomposition. The Activation energy and the preexponential factor was determined using the first-order predicted kinetics

A.4 REFERENCES

1. S. J. Lombardo and Z. C. Feng, "Analytic Method for the Minimum Time for Binder Removal from Three-Dimensional Porous Green Bodies," *J. of Mat. Res.,* **18** 2717-2723 (2003).

2. R. V. Shende and S. J. Lombardo, "Determination of Binder Decomposition Kinetics for Specifying Heating Parameters in Binder Burnout Cycles," *J. Am. Ceram. Soc.,* **85** 780-86 (2002).

3. J. W. Yun, D. S. Krueger, P. Scheuer, and S. J. Lombardo, "Effect of Decomposition Kinetics and Failure Criteria on Binder Removal Cycles From Three-Dimensional Porous Green Bodies," *J. Am. Ceram. Soc.,* **89** [1] 176-183 (2006).

4. D. S. Scott and F. A. L. Dullien, "Diffusion of Ideal Gases in Capillaries and Porous Solids," *AIChE J.*, **8** [1] 113-17 (1962).

5. D. S. Scott and F. A. L. Dullien, "The Flow of Rarefied Gases," *AIChE J.*, **8** [3] 293-97 (1962).

6. H. David, "A Review of Terminology Pertaining to Darcy's Law and Flow through Porous Media," *Journal of Porous Media*, **6** [2] 87-97 (2003).